Title

Monitoring changes in ice shelf rift propagation and infilling mélange with ICESat-2 and Landsat imagery in East Antarctica

Author

Breyer, Canyon

Publication Date

2023

Peer reviewed|Thesis/dissertation

UNIVERSITY OF CALIFORNIA SAN DIEGO

Monitoring changes in ice shelf rift propagation and infilling mélange with ICESat-2 and Landsat imagery in East Antarctica

A thesis submitted in partial satisfaction of the requirements for the degree Master of Science

in

Earth Sciences

by

Canyon Breyer

Committee in charge:

Helen A. Fricker, Chair
Adrian Borsa
Jamin Greenbaum

2023

The thesis of Canyon Breyer is approved, and it is acceptable in quality and form for publication on microfilm and electronically.

University of California San Diego

2023

DEDICATION

First and foremost, I would like to express my gratitude to my thesis advisor Dr. Helen A. Fricker for her support, guidance, and encouragement over this research journey. Her knowledge and patience in helping develop my technical, analytical, and literary skills will remain inspirational to me far beyond Scripps Institution of Oceanography.

Secondly, I'd like to thank my other committee members Dr. Adrian Borsa and Dr. Jamin Greenbaum. Their encouragement and constructive critiques advanced both this project and my analytical skills beyond what would have been capable otherwise.

I would also like to acknowledge the support of all my lab mates, cohort, and close friends who aided and supported me over the last three years. Whether it was study sessions, proofreading, journal groups, or providing a moment of clarity, being surrounded by them all was one of the greatest privileges I could have asked for.

Finally, I cannot thank my family enough. Their unwavering support throughout my schooling made this entire experience both possible and enjoyable.

EPIGRAPH

"I seemed to vow to myself that someday I would go to the region of ice and snow and go on and on till I came to one of the poles of the earth, the end of the axis upon which this great round ball turns."

Ernest Shackleton

TABLE OF CONTENTS

LIST OF FIGURES

ABSTRACT OF THE THESIS

Monitoring changes in ice shelf rift propagation and infilling mélange with ICESat-2 and Landsat imagery in East Antarctica

by

Canyon Breyer

Master of Science in Earth Sciences

University of California San Diego, 2023

Helen Amanda Fricker, Chair

Amery Ice Shelf (AIS) in East Antarctica acts as the primary buttress for the largest reservoir of potential sea level rise in the region: the Lambert-Amery Basin. Iceberg calving is an important mass loss process for ice shelf systems and is one of the ways that an ice shelf loses mass. While calving events themselves are not inherently concerning for an ice shelf, changes from the steady state such as increased

rifting and shortening calving cycles can indicate a mass imbalance. Therefore, it is crucial to understand calving processes to improve our ability to detect potential imbalances. Rifting is a precursor to all tabular iceberg calving events, yet there are many aspects of this process that remain unclear; for example, the disputed role of mélange (the ice mixture which congeals inside the rift at sea level) in rift propagation (Fricker, Young, et al., 2005; Larour et al., 2004). We use advances in satellite remote sensing to develop a metric for characterizing the propagation regime of ice rifts to indicate increased potential for calving events: the Rift Growth Metric (RGM). We determine the RGM from geometric observations derived from Landsat 8 imagery and ICESat-2 laser altimetry. ICESat-2 data enables us to characterize the status and behavior of mélange within each rift investigating its impacts on propagation of ice rifts on AIS. This method determines propagation shifts and assess mélange thickness spatiotemporally using geographic information systems software builds on established behavior of rift system dynamics before and after iceberg calving.

1 Introduction

The term “land ice” refers to any ice body which forms from the process of snow compacting into ice on continental crust and includes the Antarctic and Greenland ice sheets and glaciers and ice caps. Melting land ice directly contributes to the rising global sea level as the released water from grounded ice sheets flows into the oceans. 99.5% of permanent ice globally is considered land ice, 0.5% held as glacier ice and 99% contained in the ice sheets on Greenland and Antarctica (Vaughan et al., 2013). The Antarctic Ice Sheet is projected to become the largest contributor to sea level rise by 2050 if prevailing mass loss trends continue (Seroussi et al., 2020).

In the next sections, we discuss Antarctica and sea level rise (Section 1.1), introducing the difference in mass imbalance between West Antarctica and East Antarctica and the role of the ice shelves. Section 1.2 discusses ice shelf mass balance. Section 1.3 focuses on rift propagation on Amery Ice Shelf as a precursor to one mass loss process: iceberg calving, and has three subsections: Rift Propagation as a precursor to calving (Section 1.3.1) ; Amery Ice Shelf rift propagation (Section 1.3.2); Infilling rift mélange (Section 1.3.3). We present the hypotheses for our thesis at the end of Section 1.3.3.

1.1 Antarctica and sea level rise

Antarctica’s more than 57 meters of sea level potential lies within grounded ice sheet catchments, which flow into floating ice shelves (Fretwell et al., 2013; Rignot et al., 2019; Tinto et al., 2019) (Figure 1, next page). Antarctica’s ice shelves play a crucial role in controlling the seaward flow of grounded ice (referred to as “buttressing”), thus

slowing the rate of sea level rise (Dupont & Alley, 2005; Joughin et al., 2014; Paolo et al., 2015; Pritchard et al., 2012). However, the ability of ice shelves to buttress ice flow is diminishing due to both atmospheric and oceanic changes which have grown in signal (Adusumilli et al., 2020; Paolo et al., 2015; Pritchard et al., 2012).

Since 1979, the annual mass loss from Antarctica has increased significantly

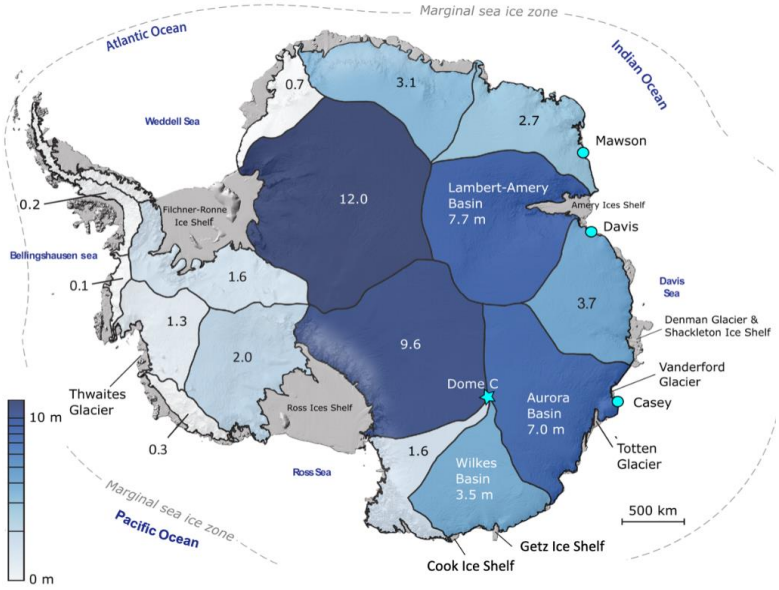

Figure 1: Antarctic drainage basins with and their respective sea level rise equivalent (Tinto et al., 2019).

from 40 ± 9 Gt/yr to 252 ± 26 Gt/yr, with the majority of the loss occurring in West Antarctica and the Antarctic Peninsula between 2009 and 2017 (Rignot et al., 2019). This has been linked to high thinning rates on its ice shelves, driven by atmospheric winds and moderated by ENSO, due to their proximity to the relatively warm circumpolar deep water (CDW) in the Pacific Sector (Adusumilli et al., 2020; Paolo et al., 2018; Rignot et al., 2019).

In contrast to West Antarctica, the East Antarctic Ice Sheet (EAIS) has maintained fairly steady mass-balance rates throughout observational history (Fricker, Young, et al., 2005; Rignot et al., 2019). A recent study by Smith et al. (2020) reported increased mass loss in Wilkes Land in East Antarctica, particularly around the Totten Glacier Basin, within the past decade. However, other regions such as the Lambert-Amery Glacier Basin and Queen Maud Land have remained relatively stable (Smith et al., 2020). While the EAIS is not experiencing dramatic mass loss like the WAIS, it is possible that the rates of mass loss for the EAIS will become more imbalanced as the global climate continues to warm, as predicted by the IPCC Sixth Assessment Report (Fox-Kemper et al., 2021). Considering that the EAIS contains nearly ten times more water than the WAIS, it is increasingly necessary to identify and understand processes indicating mass imbalance (Figure 1). Changes to ice shelves will be one of the earliest indicators that mass imbalance is imminent.

1.2 Ice shelf mass balance

Studying ice shelves requires a general understanding of all the terms involved in mass balance in the Antarctic. The mass balance of ice shelves refers to the difference between the mass accumulation of new ice and the mass ablation. The relationship between accumulation and ablation can vary greatly depending on factors such as regional geographic differences and intensity of ablation processes (Adusumilli et al., 2020; Gudmundsson et al., 2019; Rignot et al., 2019). Precipitation and the direct input of new ice from upstream of the grounding line (where the ice sheet is no longer attached to the continent and is now floating) provide the greatest mass accumulation to

the ice shelf (Adusumilli et al., 2021; Lenaerts et al., 2019; Ligtenberg et al., 2011; Walker et al., 2013). Another mass accumulation term, refreezing, occurs when seawater becomes cool enough that it can freeze to the submerged portion of ice shelves, typically closer to the ice front (Fricker et al., 2001; Whiteford et al., 2022). These mass accumulation processes provide the positive portion of the ice shelf mass balance equation.

The negative portion of the ice shelf mass balance equation includes the following mass ablation processes: sublimation, surface melting, basal melting, and iceberg calving from the ice front. In Antarctica, basal melting and iceberg calving from ice shelf fronts are the dominant processes and are believed to be responsive to interactions between the ice-ocean interface (Paolo et al., 2015; Pritchard et al., 2012). When averaged around the entire Antarctic Ice Sheet, these processes occur in roughly equal proportions; however, when considering smaller regions or individual ice shelves, the variation between dominant ablation processes increases (Alley et al., 2016; Rignot et al., 2013). On Amery Ice Shelf in East Antarctica, iceberg calving contributed more to mass ablation than basal melting (Rignot et al., 2013) (Figure 2, next page). Major calving events are infrequent, occurring in calving cycles that span several decades. Nonetheless, they are a part of the regular mass balance of an ice shelf.

Larger ice shelves such as Ronne-Filchner, Ross (West), and Amery all lose more mass from iceberg calving (Rignot et al., 2013) (Figure 2). Furthermore, iceberg calving and ice front flux dominate East Antarctic ice shelf ablation. Basal melting occurs gradually, eroding away ice near the grounding line of large ice shelves and slowly carving channels that extend from the grounding line towards the ice front (Alley

et al., 2016; Marsh et al., 2016; Whiteford et al., 2022). Large-scale tabular iceberg calving events, which are preceded by the formation and propagation of ice rifts, remove large portions of mass from an ice shelf front in a single event (Fricker et al., 2002; Walker et al., 2013). Examples of ice shelves in East Antarctica that experience iceberg calving as their primary ablation process include Cook (27.6 ± 3 Gt/yr), Mertz

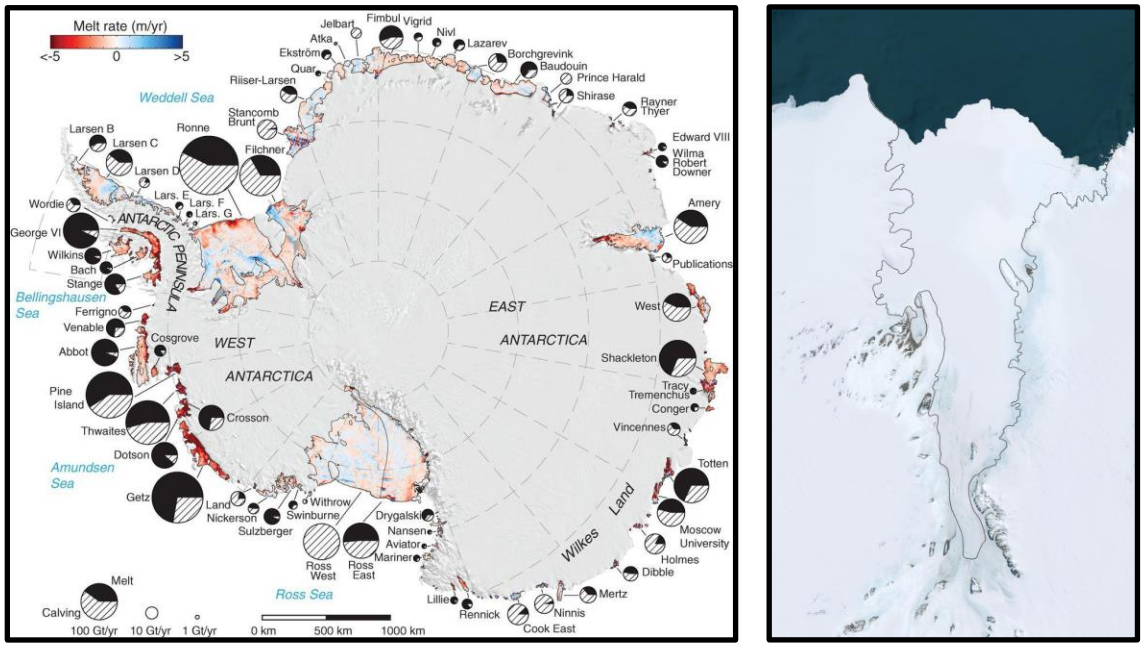

Figure 2: a) average annual mass loss from both the ice front flux (hatched) and the basal melt (solid) for Antarctic ice shelves determined by Rignot et al., 2013. Ice front flux is used proxy for iceberg calving. b) Amery ice shelf and grounding line, oriented with prevailing ice flow direction being up.

(12.0 ± 2 Gt/yr), Ross West (100.4 ± 8 Gt/yr), and Amery Ice Shelf (50.4 ± 8 Gt/yr) (Rignot et al., 2013) (Figure 2).

Calving cycles are a regular part of the mass balance of an ice shelf and can range from years to decades in length (Cheng et al., 2021; De Rydt et al., 2019; Fricker et al., 2002). The final rift propagation event which immediately precedes a calving event typically occurs suddenly over days or weeks, making prediction of these events

difficult (Bassis et al., 2005). Improved spatial and temporal resolution in satellite remote sensing enhances our ability to observe and analyze these complex processes.

1.3 Rift propagation on Amery Ice Shelf

1.3.1 Rift propagation as a precursor to calving

Iceberg calving, specifically tabular iceberg calving, is a dynamic and understudied mass loss mechanism, largely because calving events are episodic, and our satellite record is so short. However, rift propagation always precedes calving events, and it is possible to study this process in detail. Ice shelf rifts typically fall into one of two rift types: transverse-to-flow (T-rifts) and longitudinal-to-flow (L-rifts). T-rifts form perpendicular to the primary flow direction in the center of an ice shelf, while L-rifts propagate from the ice rift toward the grounding zone (Fricker et al., 2002; Phillips, 1999; Walker et al., 2013).

Rift propagation is influenced by various factors such as surface melt drainage and basal melt, which can amplify the rates of propagation (Dow et al., 2018; Spergel et al., 2021; Walker & Gardner, 2019). Because rifts through-cut ice shelves, they contain a mixture of different ice types congealed together at their base coined ‘mélange’: the mélange freeboard often lies at or just above sea level. The mélange which infills ice shelf rifts has been hypothesized to control rift propagation rates, although this has not been proven (Fricker, Young, et al., 2005; Larour et al., 2004). Rifts generally propagate over decadal time scales, but the final propagation event leading to calving is enigmatic, often behaving unpredictably and rapidly (Bassis et al., 2005).

1.3.2 Amery Ice Shelf rift propagation

On Amery Ice Shelf, most of the active rifts are longitudinal rifts, except for rift T2 (Figure 4, p. 21) . Rift propagation is described by one of four activity levels: dormant, sudden burst, intermittently active, and continuously active (Walker et al., 2013) (Figure 3, next page). We selected AIS as our study site due to its high number of continuously active rifts and the fact that it is still considered in balance (Rignot et al., 2019; Walker et al., 2013). This study builds upon previous work on rift activity and burst propagation on AIS to further investigate ice shelf dynamics (Bassis et al., 2005; Fricker, Young, et al., 2005)

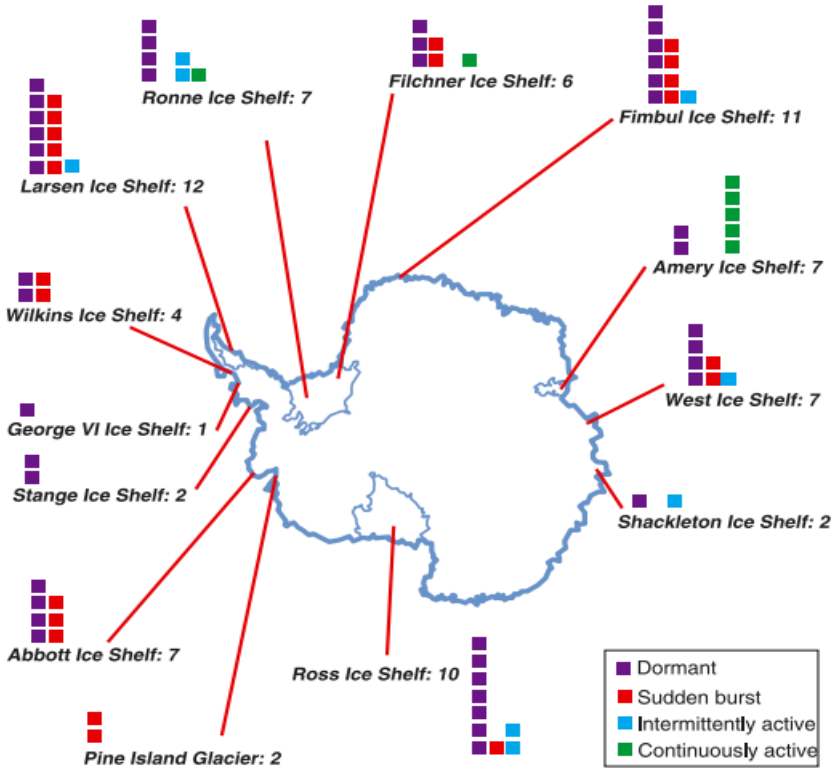

Figure 3: This map, produced for Walker et al., 2013, clarifies the distribution of the 4 major rift activity levels. Each block represents an individual rift, and the color of each respective block denotes the activity style observed.

Amery Ice Shelf contains an abnormally high concentration of continuously active rifts, most of which are L-rifts (Walker et al., 2013) (Figure 3). With its prominent topographic features and continuously active rifts, Amery Ice Shelf provides an ideal study site to assess the relationship between geometric rift evolution and changes in mélange thickness. This study aims to determine if mélange thickness influences the propagation of ice front rifts by combining data from ICESat-2 and Landsat 8 data to elaborate on the seasonal behavior of mélange and rift propagation. We demonstrate the capability of modern remote sensing techniques to detect shifts in propagation direction, which could serve as indicators of upcoming calving events.

1.3.3 Infilling rift mélange

Mélange, a conglomeration of different ice types formed at the base of through-cutting ice rifts on ice shelves, includes ice blocks from rift walls, submerged marine ice, and accumulated snow (Fricker, Young, et al., 2005; Rignot & MacAyeal, 1998). Mélange formation processes are affected by oceanic and atmospheric forcing, and its composition is not well understood. As rifts expand due to the physical stress, ice blocks from the inner wall break off and fall into the base, becoming part of the mélange matrix. The thickness of mélange tends to be greater in older or dormant rifts, but high temporal resolution observations over long periods of time are lacking (Larour et al., 2004).

Previous studies have shown the mélange generally increases in thickness over time but is believed to exhibit seasonal fluctuation as a result of warmer water exposure and increasing atmospheric temperatures from October through March (Bassis et al., 2005; Fricker, Young, et al., 2005, p. 20; Larour et al., 2021). Satellite laser altimetry

data from the first and second Ice, Cloud and land Elevation Satellite (ICESat) missions (Section 2.1) have allowed us to make estimates of mélange thickness. During the ICESat observation period (2003-2008), it was proposed that mélange may restrict the rate of rift propagation (Larour et al., 2004). An alternative hypothesis suggests that mélange formation may wedge rifts apart and contribute to rift propagation (Bassis et al., 2005; Fricker, Young, et al., 2005).

Our study investigates the two theories by analyzing spatiotemporal trends in mélange thickness and examining their correlation with geometric rift evolution. The high precision and accuracy of ICESat-2 have expanded the capabilities of remote sensing, allowing for the observation of mélange within rift walls as a well-defined cross-section (up to six observations per pass, assuming all three beam pairs record the rift). By observing ice rift propagation in two planes for each rift, lengthwise (Landsat 8) and widthwise (ICESat-2), we enhance the current understanding of seasonal mélange behavior while assessing the impacts of mélange changes on rift propagation.

2. Background

2.1 Remote sensing missions and their backgrounds for ice shelf studies

2.1.1 Monitoring ice shelf processes from satellites

Ice shelves are the floating extensions of grounded ice sheets; consequently, studying them can be difficult due to their inaccessibility. Many remote sensing techniques have been developed to circumvent this issue, including multiple satellite programs. Each satellite carries a different instrument, but most instruments fall into one of three categories.

Satellite altimeters detect the elevation of ice surfaces using laser (LiDAR) or radar-based instruments. The time between a single pulse emitted by the instrument on a satellite and the subsequent detection of the pulse reflected off of the Earth's surface is used to measure the distance from the sensor to the Earth's surface (or ice surface in our case). Both laser and radar altimeters provide elevation data, but they use different wavelengths (light for laser and radio waves for radar). The elevation measurements recorded are used to estimate ice shelf thickness changes and are also used in the monitoring of small-scale processes such as rift propagation and basal melt rate (Adusumilli et al., 2020). Laser altimeters which have been used to monitor ice shelves are the Ice Cloud and land Elevation (ICESat) and ICESat-2 (Section 2.1.2), while radar altimeters include ERS-1, ERS-2, Envisat, CryoSat-2, and the Sentinel series, which were not used here.

Optical imaging is another form of satellite based remote sensing which is regularly used for ice shelf studies. Optical sensors capture either visible or infrared images of the surface, with many modern imagery satellites using multiple instruments

in order to capture multiple spectra of light. Satellite missions such as Landsat have provided long-term imagery of the polar regions, allowing for surface feature tracking, meltwater detection, and estimation of surface elevation and ice velocity (Hambrey & Dowdeswell, 1994; Lauer, 1997; Shen et al., 2020; Spergel et al., 2021).

Synthetic Aperture Radar (SAR) instruments use microwave sensors, and the data produced can be used to map ice shelf features. SAR is particularly useful for studying polar regions because of its ability to penetrate cloud cover and operate independent of light, both of which are disadvantages for other remote sensing techniques. SAR enables detection of surface deformities, ice shelf surface velocity, and the identification of rift systems.

These remote sensing techniques, along with others have significantly advanced our understanding of ice shelves and the processes which govern their stability. By combining data types from multiple satellite missions, valuable insights regarding the behavior of ice shelves, their response to environmental factors, and the role they play in mitigating sea level rise can be determined. This study uses data from 2018-2021 from the laser altimeter ICESat-2 and the imagery satellite Landsat 8 in order to investigate ice shelf rift dynamics, so developing a better understanding of their respective mission backgrounds will clarify how we have extended remote sensing capabilities.

2.1.2 ICESat and ICESat-2 mission background

NASA’s Ice, Cloud, and land Elevation Satellite (ICESat) was launched on January 12, 2003, and operated successfully for six years, providing multi-year

elevation data for studying various environmental components. Our study, inspired by previous work published in 2005, focused on the seasonal nature of rift propagation on Amery Ice Shelf and the role of mélange thickness in rift structure (Bassis et al., 2005; Fricker, Young, et al., 2005). While the impact of mélange thickness on rift propagation has been debated, we sought to determine its contribution to the seasonal behavior. Altimeters provide an additional dimension (elevation) which passive optical sensors and some other active sensors could not achieve with the same precision (Brenner et al., 2007; Fricker, Bassis, et al., 2005). The launch of ICESat marked a significant milestone in high latitudes remote sensing.

ICESat-2 entered orbit September 15, 2018 and is still recording new observations with coverage up to 88° latitude. ICESat-2's Advanced Topographic Laser Altimeter System (ATLAS) sampling speed allows for photon data to be recorded every 0.7m with a geolocation accuracy better than 6.5m (Luthcke et al., 2021) and a vertical accuracy better than 10cm (Brunt et al., 2019). With drastically improved spatial resolution due to both sampling speed and a split beam approach compared to its predecessor, ICESat-2 expanded access to the study of small scale ice shelf processes. Ice shelf rifts are distinguishable features that can be isolated and studied effectively using altimetric data which is limited primarily by cloud cover and high roughness scales. These NASA missions have quarterly (91-day) exact repeat observations which allow for a near instantaneous cross-sectional observation of surface topography, allowing rifts and mélange to be studied more comprehensively in the last two decades.

2.1.3 Landsat mission background

The Landsat program has produced consistent satellite imagery of Earth including some of the earliest spaceborne images of Antarctica for over 50 years. The first use of Landsat imagery for Amery Ice Shelf was published in 1988 by Swithinbank which used a collection of 25 images from 1972-1974 to create a mosaic of the entire Lambert-Amery System (LAS) resulting in the identification of key surface features including flowlines and meltwater systems in the system. While originally used for better documentation of the LAS, the practicality of using visible (and eventually infrared) images for tracking features, detecting meltwater, and ice velocity estimation quickly followed.

Similarly, feature tracking through Landsat images verified that the entire LAS, including various glaciers and the Mawson Escarpment, had a consistent flow regime over the past millennium (Hambrey & Dowdeswell, 1994). This was achieved by dividing the system into eight flow units and observing the movement of specific surface features. Recent studies have highlighted the benefits of regular satellite imagery for estimating ice surface velocity and monitoring meltwater formation and drainage. Shen et al. (2020) utilized Landsat 8 imagery to produce annual ice flow maps on a 105 m grid-spacing improving the spatial resolution of data used to estimate total ice discharge around Antarctica. These ice flow maps, in conjunction with ice thickness measurements obtained from BedMachine v2, were used to estimate the total LAS ice flux (Morlighem et al., 2020; Xu et al., 2022).

Long-term imagery-based feature tracking, made possible by the increasing iterations of any satellite program, improves the capability of observing topographic

deformation processes such as the formation of surface meltwater systems and drainage features like ice dolines, reaffirming the importance of the Landsat program (Swithinbank, 1988). In this study, we use the panchromatic band (Band 8) of Landsat 8 images from 2018-2022 to track the extension rate of rift tips in the AIS rift system as a proxy for the longitudinal-to-flow rift propagation. By combining the two dimensions provided by ICESat-2 and the third dimension from the Landsat program, we analyze multidimensional changes in rift geometry and their relationship to variations in mélange thickness.

2.2 Amery observational record and calving history

The Amery Ice Shelf provides a valuable baseline dataset for monitoring Antarctic ice shelf dynamics independent of changes caused by anthropogenic forcing. The first major calving event to occur during observational history occurred in 1963 during one of the first surveys conducted on the ice shelf (W. Budd, 1966). As mentioned in section 1.1.2 (Ice shelf mass balance) iceberg calving is a natural response to mass accumulation from grounded ice flow; furthermore, it is known to follow long term cycles when an ice shelf is in steady state. Early surveys from 1968-1970 yielded the first measurements of ice velocity and strain, establishing the start of the Amery Ice Shelf historical record (W. F. Budd et al., 1982). However, traditional observational methods limited the ability to study smaller scale processes such as rift propagation and mélange thickness.

In recent decades, the increasing availability of satellite data has improved accessibility for documenting calving events and developing a better understanding of

the Amery Ice Shelf calving cycle. Fricker et al. (2002) identified the triple junction rift system, now referred to as the “Loose Tooth” (LT) comprised of a longitudinal rift and two traverse rifts (T1 and T2), to describe the Amery Ice Shelf calving period using a 1963 image from the Corona satellite mission and comparing it with the status of the LT system to predict a calving cycle of 60 years. Following the identification of this triple junction, the study of the continuously active rifts began. Further research revealed that the LT rift propagation was episodic and that background glaciological stress was the primary driver of rift propagation on the Amery Ice Shelf, while environmental factors such as prevailing wind and tides only significantly impact propagation just prior to calving events (Bassis et al., 2005).

The second major calving event to occur in observational history was more recent, allowing for an in-depth study of the rift behavior leading up to the formation of iceberg D-28. D-28 was calved in September 2019 and was 1,646 square kilometers (roughly the size of the Hawaiian island, O’ahu) (Walker et al., 2021). This calving event provided a second data point making the observed calving cycle roughly 60 years, confirming predictions made in Fricker et al., 2002. The calving occurred following a significant acceleration of the propagation rate of rift T1 at the ice front (the western branch of the “Loose Tooth” rift system). ICESat-2 data revealed traces of propagation through subtle (~1.0m) topographic signatures of the rift that satellite imagery from Landsat-8 had been unable to resolve (Walker et al., 2021). This recent calving event serves as a valuable example for how understudied the processes involved in rift propagation remain.

2.3 ArcGIS Pro and Spatiotemporal Analysis

Esri (formerly the Environmental Systems Research Institute) was founded in 1969 and provides geographic information systems (GIS) software. With hundreds of analytical tools and the ability to use both vector and raster data, the ArcGIS Pro software allows users to conduct their own geospatial analyses to produce meaningful results for any spatial data.

In this project, we primarily use the Space Time Pattern Mining toolbox which contains tools designed for spatiotemporal analysis and calculating results which describe the clustering intensity of the relationship between individual data points and their neighbors (both spatially and temporally). These tools, as well as others outside the Space Time Pattern Mining toolbox that were used are detailed in section 3.4.2.

There were two major benefits to using ArcGIS Pro for spatiotemporal analysis. First, the software provides powerful data visualization capabilities. These include both 2D and 3D scenes. By visualizing the data with the proper geographic reference and allowing for easy conversion between multiple geographic reference systems, we gain better context for the importance of accurate data processing and are able to visually verify any data corrections made. By easily transforming all data into the same projection, such as the South Pole Lambert Azimuthal Equal Area Projection (SPLAEA) in our case, ArcGIS allows us to ensure consistent visualization. While the typical Polar Stereographic 71 projection was considered, we decided to use SPLAEA because it maintains the true relative size of land features, working well for topographic features

such as rifts in our case. This emphasis of visualization promotes the use of map-based figures, improving the geographic context of analytical results.

Second, ArcGIS Pro offers hundreds of predeveloped and statistically robust tools, allowing us to select the most suitable geospatial analysis methods to answer our research questions. The choice of the Space Time Pattern Mining toolbox allows us to investigate spatiotemporal trends of ICESat-2 data to deepen our understanding of rift dynamics by examining the relationship between ice mélange thickness and surrounding rift growth rates.

3. Data and Methods

3.1 Data

3.1.1 ICESat-2

ICESat-2 data was downloaded in the preprocessed Land Ice Along-Track Height Product from the NSIDC (Hierarchical Data Format version 5 [HDF5] file format) or from OpenAltimetry (csv file format) (Smith et al., 2019; Khalsa et al., 2020). For the three rifts targeted in our study, ICESat-2 observations were only plotted if the track data were clear (no perturbations due to cloud cover) for a given date. When necessary, we converted the data from the HDF5 file format into a csv format using h5py and pandas packages so that all ICESat-2 data was in csv file format which allows for easier management in ArcGIS Pro, but much of our data from Open Altimetry was able to be downloaded in this format. Following this conversion, we filtered the data down to the necessary components: latitude, longitude, trackID, h_li (the elevation above the ellipsoid), and the file name. Using the file name, a new date-time field was created in the converted csv files in order to maintain the temporal component of each data point. Finally, the number of days between true observation and June 21, 2020 (the temporal midpoint of our study period) was calculated and added as a final data field for use during ice advection removal later (Section 3.1.3). By adjusting all observations to the temporal midpoint, we are able to minimize any potential error or discrepancies in ice velocity.

3.1.2 Landsat 8 Imagery

One of the geometric parameters considered was the rate of longitudinal rift extension (Figure 4, p. 19). For this, we used Landsat-8 images over the study period (2018-2022) and used band 8 (panchromatic) which has the highest spatial resolution at 15x15m. We chose to simply use band 8, rather than pan sharpening the visible imagery because we did not rely on a high degree of spectral resolution to identify the rifts, we simply needed the highest spatial resolution possible. Furthermore, we only used images with less than 10% cloud cover which makes consistently locating the rift tip in images more possible. In order to decrease uncertainty in rift tip identification in Landsat 8 images, we adjusted the gamma value of each image to reduce and standardize manual measurement color bias. The gamma value represents a pixel's luminosity and by adjusting this value we can fine-tune the brightness and contrast of a given image. By increasing the gamma value shadowed details are enhanced; alternatively, by decreasing the gamma value details of the brighter areas in the image are revealed as the mid-tones darken.

3.1.3 Data Corrections

The following corrections were performed to the ICESat-2 ATL06 elevation data:

Geoid offset proxy: When investigating mélange, the elevation data recorded by ICESat-2 is really the freeboard. Because the entire system is floating, later calculations from mélange freeboard to estimated thickness require the ICESat-2 data to be referenced to the geoid. We used a proxy for the geoid offset by measuring the average

elevation height in the ocean beyond the ice front (either sea ice or the open-ocean surface dependent on time of year) for the entire study period, and subsequently subtracted this height (14.3 m) from our data as a conversion from observed elevation above the WGS-84 ellipsoid to estimated elevation above the geoid (or mean sea level). By applying this proxy offset, the elevation data is represented as meters above local sea level. .

Tide correction: The entire ice shelf responds instantaneously to the ocean tide, and the tidal amplitude at the time of the ICESat-2 pass must be removed to account for this (Fricker and Padman, 2006). The CATS2008 Tide Model was used to create a new data layer for the specified extent of each rift which was then subtracted from our filtered ATL06 so there was no tidal signal in our data.

Ice advection: To consider how changes occurred locally within a specific rift system, it was important to remove the advection of the ice shelf in order to return an observed point to the expected position if the system was not flowing. By creating a Lagrangian system for each rift through this correction, we avoided binning inconsistencies and analyzed the data as though each rift was stationary. We completed this using MEaSUREs-2 Ice Velocity data and moved each track forward or backward in time to the corrected geographic position (Rignot et al., 2017).

These corrections allowed for removal of both vertical and horizontal displacements due to predictable external influences ensuring that changes in rift wall position are at least partially indicative of true propagation, and that changes in mélange

elevation were a result of thickness changes. Details on estimating mélange thickness are included in Section 3.2.3.

3.2 Amery Ice Shelf rift classification (study site selection)

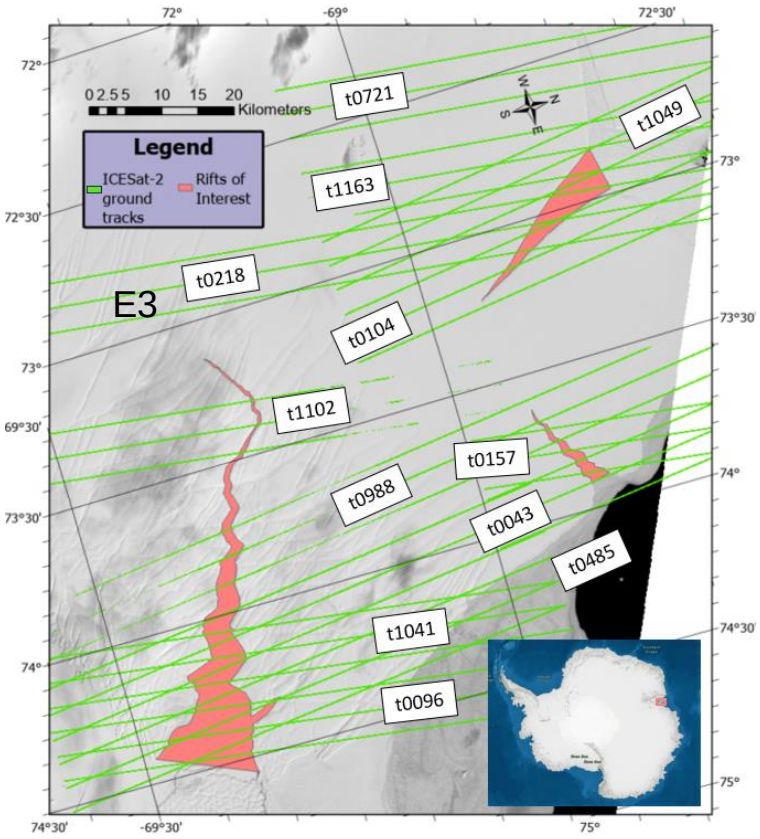

Figure 4: Amery Ice Shelf rifts T2, L2, and E3 were the focus of this study due to their continuously active status, variable rift type (longitudinal and traverse), and their presence on an ice shelf that has experienced recent a major recent calving event (Walker et al., 2021). (Landsat 8 Acquisition Date: January 20, 2020)

Studying stable locations in Antarctica allows investigation of ice shelf processes rather than the climate-driven trends impacting other places (King et al., 2009). In this study, we selected three rifts (L2, E3, and T2; Figure 4) for the following reasons:

(i) Based on the activity level classification established by Walker et al. (2013), these rifts are continuously active. Continuously active implies that the rifts undergo some

degree of propagation every year. Therefore, they are more likely to exhibit noticeable growth over the study period.

(ii) This set of rifts includes both longitudinal and traverse rift types, allowing us to investigate the relationship between mélange thickness and rift geometry for each separately.

(iii) These rifts are located near a recent tabular calving event (D-28 in September 2019). The proximity to this event is relevant for two reasons: First, an iceberg calving usually implies an extended period before the next calving event; second, it offers an opportunity to study the impacts of tabular calving, which is inherently sporadic, on the surrounding system. With one year of seasonal ICESat-2 data before the event, and over two years of data after it, we observed changes in propagation rate leading up to the calving event and its impact on the local rift system.

These unique traits make AIS rifts L2, E3, and T2 a diverse selection, ideal for studying the behavior of rift growth concerning mélange thickness.

3.3 Rift parameters used for monitoring

All three of the rifts in this study (L2, E3, and T2) now propagate from the ice front landward and are considered continuously active, but vary in their rift propagation direction (L for longitudinal, T for transverse). To best characterize the growth of each rift, two different geometric parameters were investigated: rift extension (longitudinal-to-flow propagation) from the tip to the rift mouth, and rift width widening (transverse-to-flow) from the one side of the rift wall to the other (Figure 5). Using both geometric

parameters to build a multidimensional metric for rift growth, the hypothesis that the mélange base may act as a control for rift growth by comparing mélange thickness changes analyzed spatiotemporally to local geometric growth could then be tested (Figure 5).

3.3.1 Rift length for longitudinal-to-flow propagation

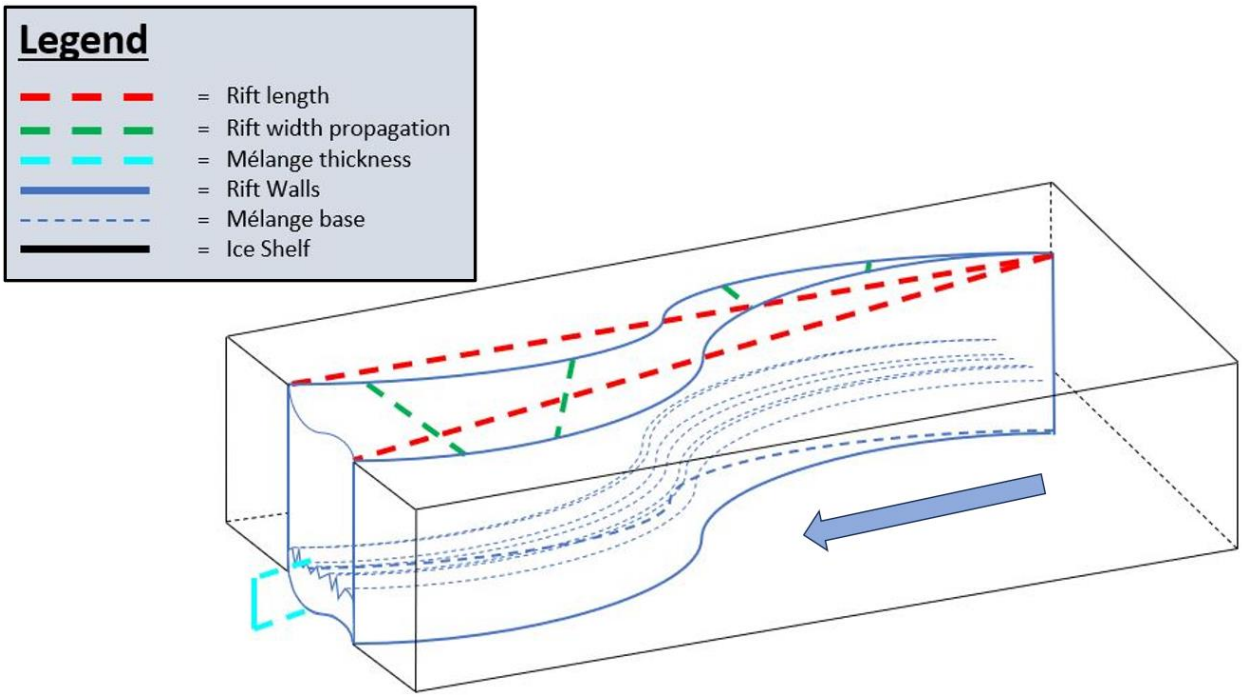

Figure 5: We consider 2 geometric parameters, rift length (red) and rift width (green), and one physical characteristic (mélange thickness (blue)) for each rift to help determine the style of rift growth and determine if mélange acts as a control on rift growth on the Amery Ice Shelf.

To capture the change that occurred on one plane in an individual rift system, we measured the longitudinal-to-flow rift extension. Rift length was measured manually in ArcGIS Pro using Landsat-8 images by taking the average of the distance from the rift

tip to the easterly and westerly edges of the rift mouth at the ice front measured in meters (Figure 5). We used the panchromatic band images (band 8) because the manual measurement method relied more heavily on spatial resolution than upon spectral resolution. Because we did not need such a broad span of spectra, we could use an imagery band with higher resolution. For each successive image, the number of days between each observation was used to calculate the instantaneous rate of longitudinal rift extension, providing the first geometric parameter needed to improve our understanding of rift growth.

3.3.2 Rift width for transverse-to-flow propagation

We also investigated a second geometric parameter along an alternate plane; the rate of rift widening. ICESat-2 provides a cross section of a rift with each cloud-free pass providing a snapshot of the rift walls and mélange thickness (Fricker, Bassis, et al., 2005; Fricker et al., 2002; Walker & Gardner, 2019). The rate of widening serves two purposes: first, it provides an instantaneous estimation of the lateral growth rate of a rift used to help predict potential calving events; second, it further informs the seasonal nature of rift propagation (even for rifts classified as continuously active) (Fricker, Young, et al., 2005; Walker et al., 2013). We removed repeat tracks inhibited by the presence of clouds, which obscure the laser path from the ATLAS instrument. Subsequently, data was filtered to only include measurements between 0m and 200m above the geoid which would remove any ambiguity from minor atmospheric disturbances while still preserving points that exist on or above the geoid (sea level). Due to data loss driven by complications from cloud cover, ICESat-2 collects an

inconsistent amount of cloud-free observations seasonally. We clarified the number of successive observations (repeat within 2 cycles) collected for each reference ground track (RGT) over the study site and found that repeated observations happen more prevalently in the summer and fall months (austral winter) (Figure 6). During this time period in the southern hemisphere, cloud cover typically increases drastically and often rift propagation will reduce substantially (to a near standstill in most cases) (Bassis et al., 2005; Fricker, Young, et al., 2005). Successful observations in the summer months allowed us to capture the final position of the rift before the austral winter period, while

successful observations in the fall months (austral spring) allowed us to capture the earliest position of each rift before the major propagation period annually.

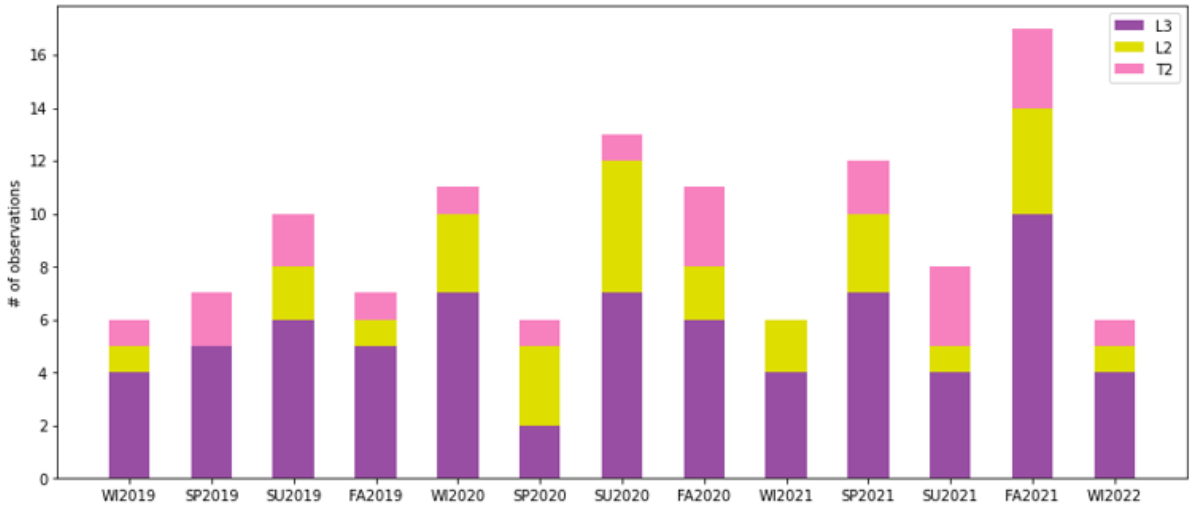

Figure 6: ICESat-2 has a 91-day repeat providing seasonal observations of the Amery Ice Shelf. Here, separated by color, the number of successive repeats (two observations within 91 or 182 days of each other) used to determine the along-track propagation. The difference in total observations of each rift is due to the varying rift size where L3 is much larger tin extent than L2 or T2. It was found that summer and fall have the highest concentration of successful repeat observations.

To estimate along track propagation, we plotted all cloud-free cycles for each RGT (Figure 7). We measured this widening rate for all tracks which contact each rift (E3: 15 tracks, L2: 6 tracks, T2: 5 tracks) and along each viable beam (~6 beams per observation). We removed tidal fluctuation using the CATS2008 Tide Model and approximated the advection correction to cycle 8 using ice velocity from MEaSUREs v2. These corrections allowed us to remove natural fluctuations in position caused by the behavior of the ice shelf and the ocean beneath, thus allowing us to treat each rift as its own independent Lagrangian-style coordinate system. By assessing each rift independently, we preserved the intrarift variation while accounting for system-wide movement. Finally, the widening rate determined by measuring the seasonal change in

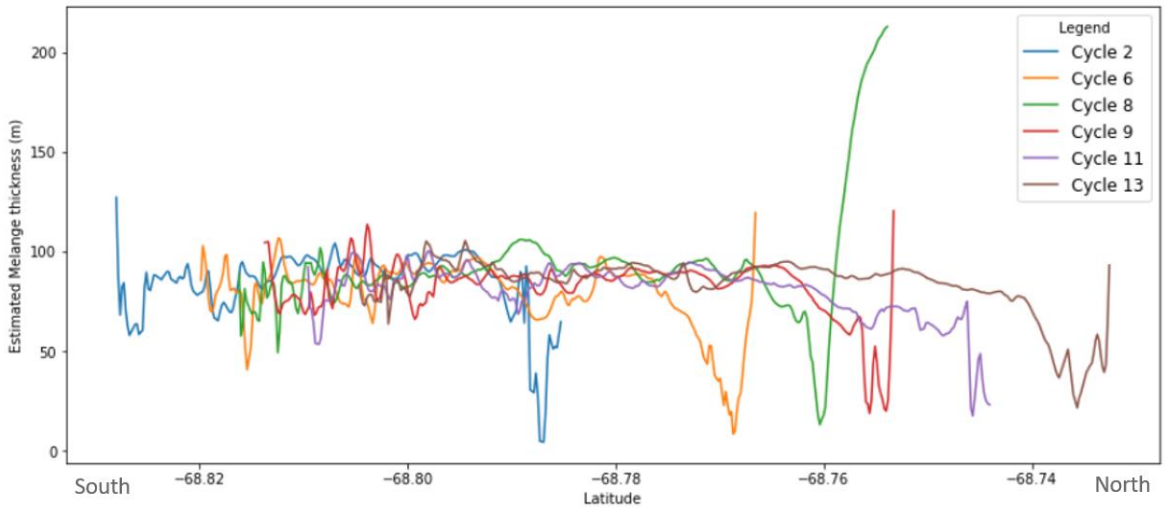

Figure 7: Beam 2l for rgt 0218 processed data for approximated mélange thickness over rift T2 which shows the windblown side (left) of the rift with thicker mélange and the opposite side with a rapid decrease indicating the propagation of the northern (right) rift wall.

observed rift width taken from ½ the average rift depth. By observing the rift width here instead of at the base of the inflection point of the ice shelf surface into the rift, we

remove any ambiguity that may be caused by surface melting or mélange changes near the rift walls. This technique also excludes the potential for new blocks of ice which may calve from the inner rift wall and fall into the mélange base to make the rift base appear artificially smaller (Walker et al., 2019, Figure 7).

3.3.3 Rift Growth Metric (RGM)

With both rift geometry parameters (longitudinal extension and rift widening), we investigated the rift growth from both an intrarift and interrift perspective. We aimed to gain a comprehensive understanding of the behavior of individual rifts independent of their ice shelf system by analyzing geometric growth patterns. Additionally, we investigated whether rifts exhibit behavior independently, or if certain events, such as the calving of D-28, influence rift growth beyond the individual scale. We developed a new metric for rift growth called the Rift Growth Metric (RGM), the ratio between the average extension rate to average widening rate for each rift. By indicating the primary style of rift growth, either longitudinal-to-flow or transverse-to-flow, we provided better characterization of ice shelf rift evolution.

3.4 Using ArcGIS Pro to estimate mélange thickness and behavior

3.4.1 Mélange thickness

In order to estimate mélange thickness from ICESat-2 elevation above the geoid, further correction was necessary. First, we reduced the data to only the recorded elevation points contained between rift walls, so the only data used was taken on

mélange or open water by creating a polygon within ArcGIS Pro which follows the rift walls. We identified the rift walls by detecting the variance within 500 m windows and symbolizing the data to show large, localized elevation drops of 20-30 m where variance was exceptionally large. However, we were still simply looking at the mélange elevation above sea level (freeboard). To estimate mélange thickness, we used Archimedes principle assuming no snowpack and assuming no overall change in mélange density (Fricker, Bassis, et al., 2005). Now that mélange thickness had been estimated, we used ArcGIS geospatial tools to prepare our data for space-time pattern mining. As each of our data points has its observation date tied to it already, we combined all of the data tracks from each locality into a site-specific data layer so that a STC for each rift in the AIS system could be created. We chose to work with individual STCs for each rift because it allowed us to observe each rift independently, and because their mélange thickness varied greatly so no single classification scheme proved viable across the entire AIS rift system. The final step in the data preparation for the space-time pattern mining was to project the dataset using a South Pole Lambert Azimuthal Equal Area Projection (Figure 8). Ideal for data restricted to a single hemisphere, this projection maintains the true relative size of large topographic features making it a reasonable choice for the AIS rift system; moreover, STCs require projected datasets for input.

3.4.2 Space-Time Cube creation and Emerging Hot Spot Analysis

Now with the data properly filtered, we made the first major step in our spatiotemporal analysis of mélange thickness. We aggregated the processed ICESat-2 point data into hexagonal bins of 1000 m distance intervals. We used a time interval of 3

months; treating the equinox or solstice which occurred most recently prior to the first ICESat-2 observations as the reference start time (September 22, 2018). I employed a hexagonal grid binning system, where (within each bin) the median mélange thickness estimated from elevation above our geoid offset proxy (section 3.1.3) was measured by ICESat-2 observations (h_li) and any missing data due to poor quality or cloud cover was replaced with zeroes. While other options for filling Null data exist, the only other readily available option involves filling Nulls with interpolated temporal neighbors which have no spatial component. Typically, cloud cover restricts the use of an entire data track when present, so spatial neighbors are too sparse for reliable interpolation. Providing the first look at the spatiotemporal variability of mélange thickness, we use the "Visualize Space-Time Cube in 3D" tool to build a new map in which our recently created STC for ice rift mélange thickness could be examined in 3 dimensions (Figure 8). In the STCs, color represents the median elevation within each bin over the specified time interval (seasonal). The vertical component in this case is time. Furthermore, as the color of a particular column changes over time, it provides a visual representation for the seasonal changes of mélange thickness in each 1000m locality.

Finally, now that the STC was created, we needed to determine the spatiotemporal patterns within the cube itself. The "Emerging Hot Spot Analysis" (EHS) tool performs three analyses on each column of the STC resulting in a localized classification of the spatiotemporal variability of the mélange thickness. First, each bin was analyzed with respect to its spatiotemporal neighbors by calculating the Getis-Ord Gi* statistic to measure the clustering intensity of mélange thickness change within the rift and a z-score and p-value are calculated. One of 17 different binning categories was

assigned to each bin in the STC. We then evaluated the time series of the clustering z-scores derived in the first step of the analysis using the Mann-Kendall statistic (Mann-Kendall and Getis-Ord Gi*) resulted in the identification of local changes in mélange thickness and ultimately allowed for comparison between mélange thickness and rift growth changes to more accurately characterize their relationship.

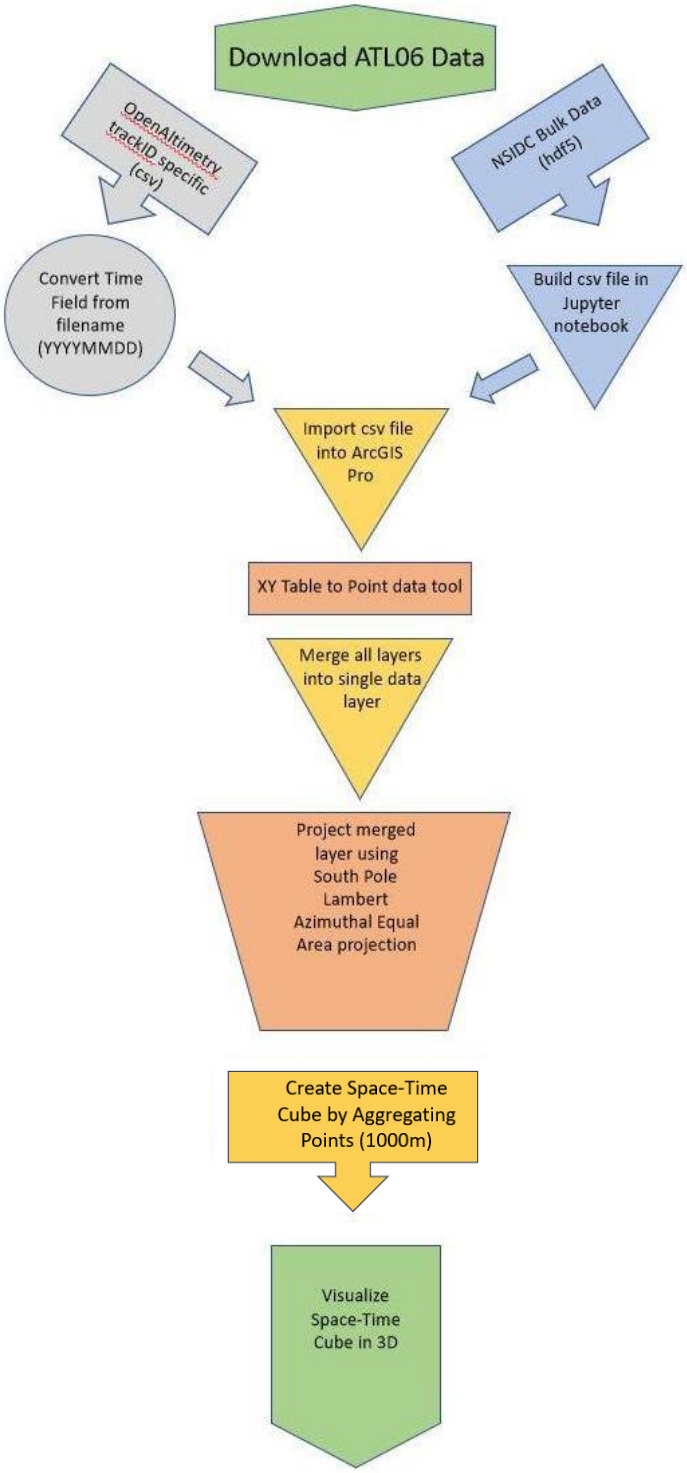

Figure 8: The simplified workflow utilized to build a Space-Time Cube in ArcGIS Pro from ICESat-2 data. Note the input data should be in csv format with coordinates for all data points, and that the tool requires a projection to be applied.

4. Results and Analysis

Following the order set by our Methods, we will first cover the geometric growth results relating to propagation styles. Next, we will elaborate on the RGM and the implications it may hold for calving prediction. Finally, we will conclude with Space-Time Cubes and the Emerging Hot Spot Analysis that we used to investigate ice mélange, and its relation to ice shelf rifting.

4.1 Geometric Results

4.1.1 Rift Lengthening

We manually determined the rate of longitudinal extension for rifts T2, L2, and E3 on Amery Ice Shelf from gamma-adjusted cloud free images collected by Landsat-8 over our study period (September 2018 – March 2022). The measurements were collected by determining the point farthest upstream from the ice front at which a rift

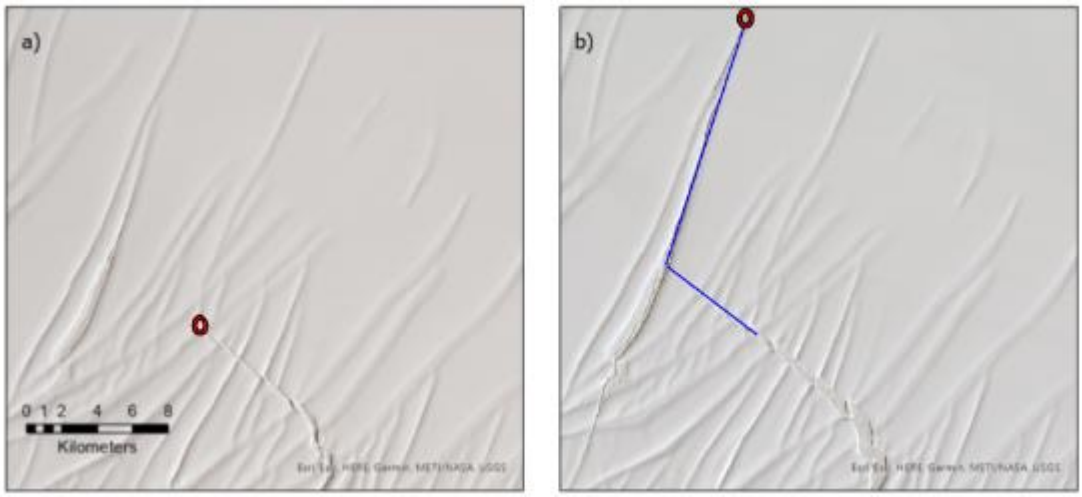

Figure 9: Landsat 8 captures these two natural color images of the upstream rift tip of the E3 rift system on AIS. The images were taken on September 27, 2018, and December 1, 2021, respectively

could be identified and averaging the distance from this “rift tip” to each edge of the rift mouth in each image (Figure 5).

Along this propagation plane (extension plane) rift E3 behaved differently from T2 and L2. Over the study period, the rift extended over 23 kilometers upstream while connecting with an additional rift (Figure 9). In contrast, rifts T2 and L2 propagated less than two kilometers along their respective extension planes. E3 propagated rapidly each melt season, the largest propagation seasons occurring following the D-28 calving event detailed in Walker et al., 2021. Over the 1,161 days between the images used in Figure 10, E3 extended 23.14 km resulting in an extension rate greater than 20 meters per day; substantially faster than the extension rates of T2 and L2 whose extension rates remained generally below two meters per day (Figure 10). In addition to the strong domination of extensional growth in E3, we note that the increase in extension did not

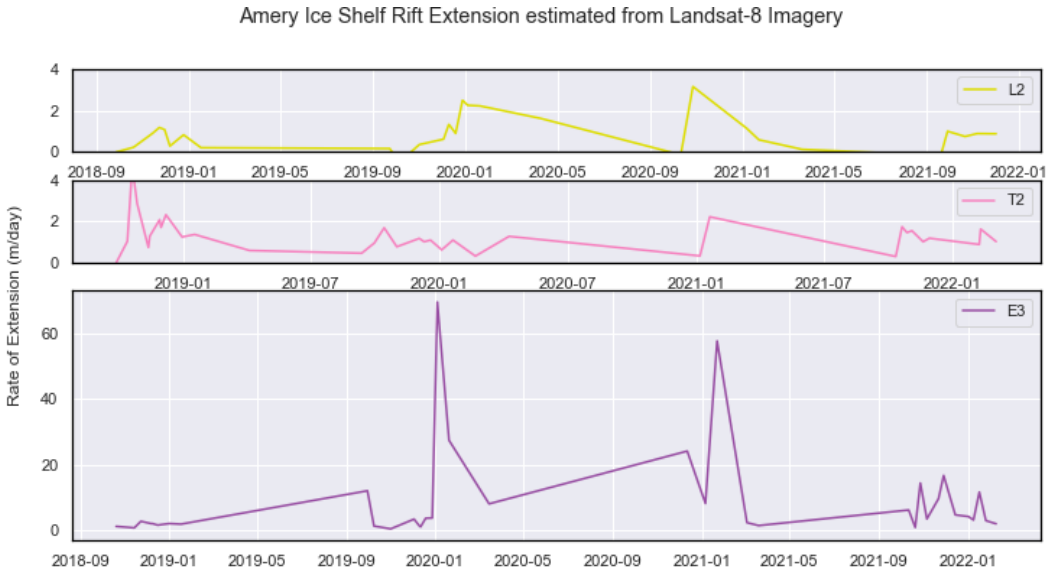

Figure 10: The longitudinal rate of extension for each of the three rifts was measured as portrayed by Figure 5 using available Landsat 8 images with 0-10% cloud cover over 14 ICESat-2 cycles (42 months) from Septemeber 2018 through March 2022

become notable until the Landsat 8 images which followed the D-28 calving event in September 2019.

Another relevant observation we made derived from the intensity of extension ultimately following the initial increase for E3, propagation rates decreased each subsequent season (Figure 10). Despite the scarcity of cloud free images throughout the Antarctic accumulation season (March – August) our longitudinal-to-flow results are consistent with Bassis et al., 2005 and Fricker et al., 2005b, noting that the rift tip typically remained stationary or near stationary (less than 1 meter per day) throughout these periods (Figure 10). While these studies aided in confirming that seasonal propagation occurs naturally and independently from environmental forcings, we aim to show that mélange thickness changes are regularly coupled with propagation changes.

4.1.2 Rift Widening

The second geometric parameter observed in this study was rift width propagation estimated using successive observations of elevation collected by ICESat-2. We restricted our propagation rates to include observations which occurred within two repeat periods of each other (182 days). Despite its unmatched accuracy and precision, ATLAS's 10-cm vertical uncertainty and 5-meter horizontal uncertainty can only provide seasonal high-resolution observations (Brunt et al., 2019; Luthcke et al., 2021). Therefore, we use all 6 beams on each successful observational pass to increase the spatial resolution as much as possible. Treating each rift as an independent Lagrangian coordinate system, we can better visualize how each rift propagates regardless of the overall system. We found the rift mouth (located at the ice front in all three cases) typically experienced greater transverse-to-flow propagation rates than the upstream areas of the rift in more active rifts (T2 and E3). Additionally, we again found the same seasonal signature noted in the longitudinal-to-flow observations (higher rates over the

melt season, lower during the accumulation season) remained consistent for this plane of propagation. Considering an individual track, it becomes more clear (after applying Archimedes principle to estimate mélange thickness assuming no snow pack) that the quickest transverse-to-flow propagation occurs in locations where the local mélange thickness grows. In this case, local refers to along-track within two cycles. Adding further evidence regarding mélange thickness advancing rift propagation, we confirm using these ICESat-2 observations that rifts T2 and E3 experienced higher rift width propagation coupled with thinner overall mélange thickness as the only major characteristic difference between these rifts and rift L2.

4.1.3 Limit of rift detection by ICESat-2

To determine the limit of ATLAS's capability for detecting rifts and place a lower bound on the application of ATLAS for rift detection, we also searched for the minimum detectable rift width in the ATL03 data. Using the rift catalog provided by Walker et al., (2013) as a guide, we used OpenAltimetry to find the narrowest profile which included rift walls on both sides of the rift, and observations of the surface of the infilling mélange. We overlaid these elevation measurements with the Landsat-8 image acquired on the date closest to the ICESat-2 observation.

This overlay allowed us to confirm the existence and size of a rift in a recorded ground track as well as provide visual context for the vertical dimension for ICESat-2 elevation data. The best case of a rift observed with both rift walls and the infilling mélange was recorded along RGT 0104 on September 29, 2021 (Figure 12). Using ArcGIS Pro to overlay the track data on the georeferenced Landsat-8 image from the

consecutive day, we clearly identified the rift as well as the mélange filled base with 10 photon measurements from NASA's ATL03 raw photon data product for ICESat-2 between the rift walls. This identification was done by filtering ATL03

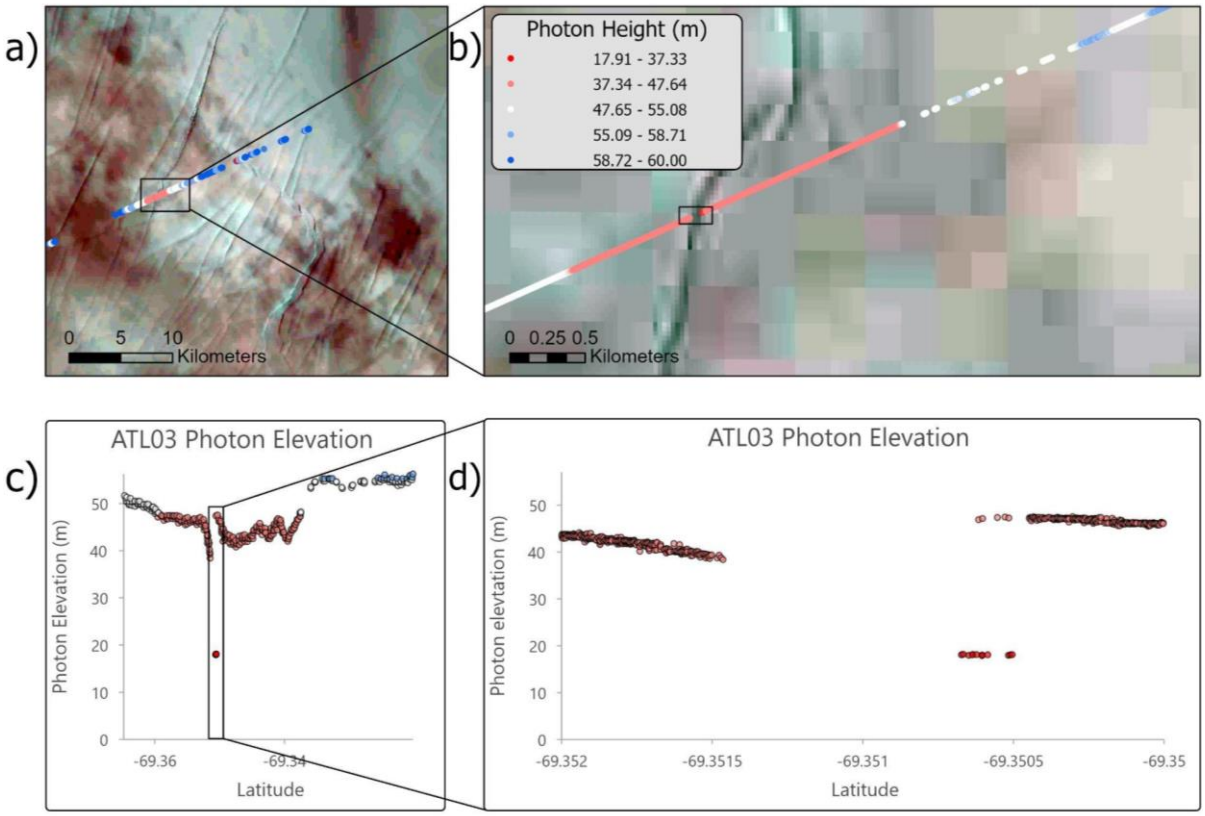

Figure 11: This observation is from track 0104 beam 1gtr recorded September 29, 2021. This is the narrowest recording of a rift and its mélange that we were able to find by ICESat-2. a) and b) are an image acquired by Landsat-8 on September 28, 2021, and photon height is symbolized to emphasize the presence of the rift with red representing the mélange base. c) and d) show the same track in the vertical dimension. 10 photon measurements over 18.7 meters confirm a mélange base within a rift.

data to only include photons with a high or medium confidence classification and subsequently symbolizing the recorded photons by elevation where red points portray measurements recorded significantly below the surrounding topography and blue points portray those significantly above the surrounding topography. While cases of minor

surface topography indicative of rift formation have been recorded to the resolution of ~1 m, these recordings exclude rift walls or mélange (Walker et al., 2021). We used this rift observation to confirm that rifts 20 m or wider can successfully be recorded by ICESat-2 retaining a small signature in the Land Ice Along-Track Height Product, with a 20 m resolution, and remain pronounced in the raw photon data.

4.2 Rift Growth Metric (RGM)

We gain important insight into the behavior of rifts by considering a new metric for rift growth, determined by the combination of both extensional and width-wise propagation (two plane propagation). As shown by many others (Fricker, Young, et al., 2005; Lipovsky, 2020; Rignot & MacAyeal, 1998; Walker et al., 2013), rifting precedes large-scale tabular calving events. Additionally, the behavior of rifts and the subsequent calving remains unpredictable due to the rapid and episodic nature of rift propagation that typically occurs just before calving (Bassis et al., 2005). Rifts may initiate decades or even centuries before they ultimately lead to a calving event, however the above behavior establishes rapid longitudinal-to-flow propagation as the most prominent propagation style immediately before calving.

By taking the ratio between the transverse-to-flow propagation to the longitudinal-to-flow propagation, we characterize, within a 3-month period of uncertainty, when a particular rift switches primary propagation styles from being transverse-to-flow dominated (like L2 and T2) to longitudinal-to-flow propagation (like E3): this regime change indicates a higher likelihood of continued propagation and ultimately tabular calving events. Due to the temporal resolution of our data, while we cannot resolve any

signal at a finer scale than 3 months, we still are able to discern an annual RGM signal in which longitudinal-to-flow propagation becomes more prevalent (increased RGM) through the ablation season (Figure 12).

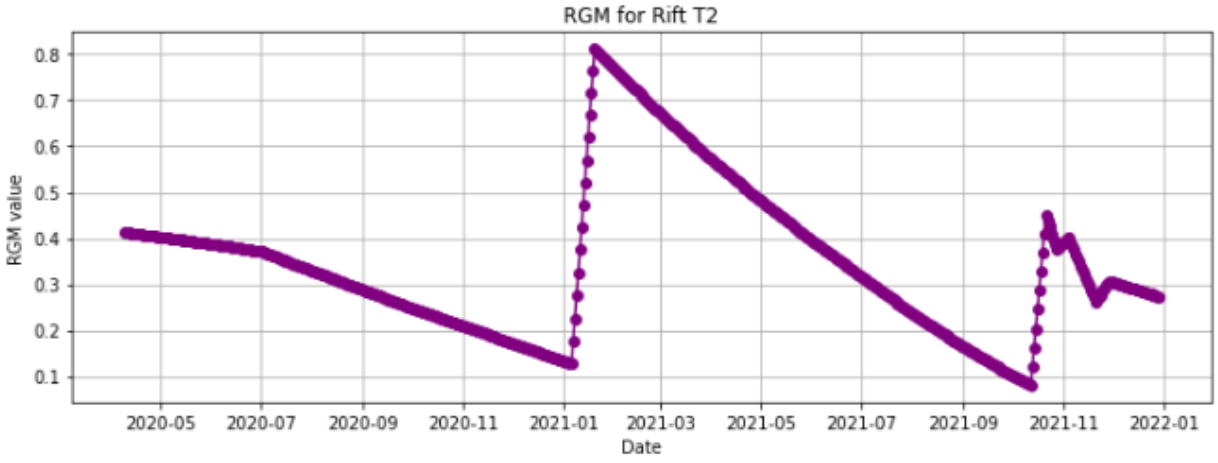

Figure 12: By taking the ratio of the rate of extension to the along-track rift widening rate, we gain a better understanding into the primary propagation method of each rift. Rift T2, maintains an RGM lower than 1.0 showing that it is currently dominated by along-track rift widening. Annual spikes which approach an RGM of 1.0 add further credence to the seasonal propagation of Antarctica's ice rifts.

4.3 Spatiotemporal analysis of mélange thickness

4.3.1 Seasonal variation of mélange

To investigate the seasonal nature of mélange surface change in Amery Ice Shelf active rifts, we first approximated mélange thickness as outlined in section 3.4.1. By accounting for advection to effectively move each ICESat-2 observation forward or backward in time (minimizing the degree of error any particular track would be subject to), we were able to capture roughly seasonal observations of the mélange base of each rift in our study. We then were able to compare the seasonal mélange thickness approximation finding that each rift did experience some seasonal variation (Figure 13).

This is the first confirmation of the seasonal nature of mélange thickening in Antarctic accumulation seasons (June to September) and thinning in Antarctic ablation seasons (December-March).

It is evident from the rift lengthening and along-track widening rates that rift L2 is the least active, and relatively stable histogram structure throughout the 14 cycles. We also note the greater approximate mélange thickness in this older and less active rift, with averages between 91m and 96m, consistent with results from Larour et al., 2004. Consequently, we also noticed that this rift being the least active behaved irregularly compared to the more active T2 and E3. For rift L2, we found that summer mélange thickness was the thickest average, when we would likely expect the mélange surface to be thinning. This can be explained by two factors: the drastic decrease in observational capacity during winter months when cloud cover is more prevalent, and the small size of rift L2 making the total number of observable tracks relatively small compared to T2 and E3.

In rifts T2 and rifts E3, the total amount of observations increased drastically allowing for more reliable interpretation of the mélange distribution. We found that the position of seasonal means was reasonably consistent with our expectations with the thinnest approximated mélange thickness occurring in summer and remaining thinner until the accumulation season in winter where the thickness would increase to its annual high. Upon separation of each season into individual histograms (rather than overlaid), we also found that rifts T2 and E3 had more definitive peaks in each season, while rift L2 either had multiple peaks or roughly uniform structure.

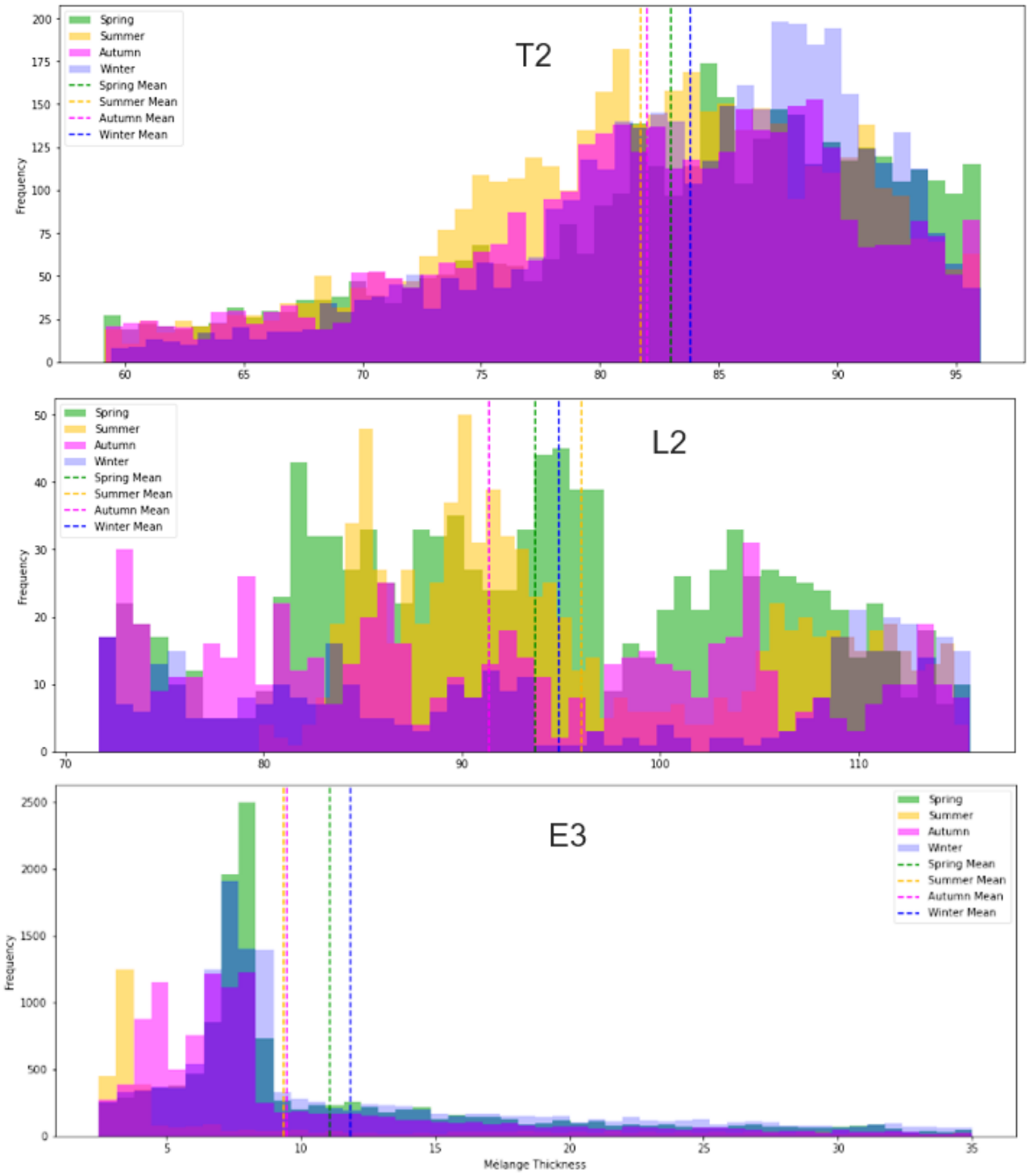

Figure 13: The distribution of observed mélange for each of the three rifts split by austral seasons (for example, summer months indicating December 21 - March 20 annually and winter months indicating June 21 - September 22 annually). By also displaying the mean of each distribution, we can see the seasonal variation in mélange thickness. Note that these histograms cut the lower and upper 10% of data from all observed mélange to remove outliers.

4.3.2 Space-Time Cubes

Our results were consistent with those of Fricker et al., (2005b), reaffirming that mélange thickness varies seasonally, but also illuminating the previously unrepresented lack of uniformity in mélange thickness over the extent of a particular rift. We used a Space-Time Cube (STC) to visualize the evolution of each rift's mélange base accurately and concisely over the course of the study period, as derived from ICESat-2 data. Each column represents a 1000m locality and the bins within a column represent each seasonal observation (bottom to top, oldest to newest). Our results indicated the thinnest mélange for ice front-initiated rifts exists at the ice front and the thickest near the rift tip (Figure 14). The Space-Time Cube displayed in Figure 14 best exemplifies

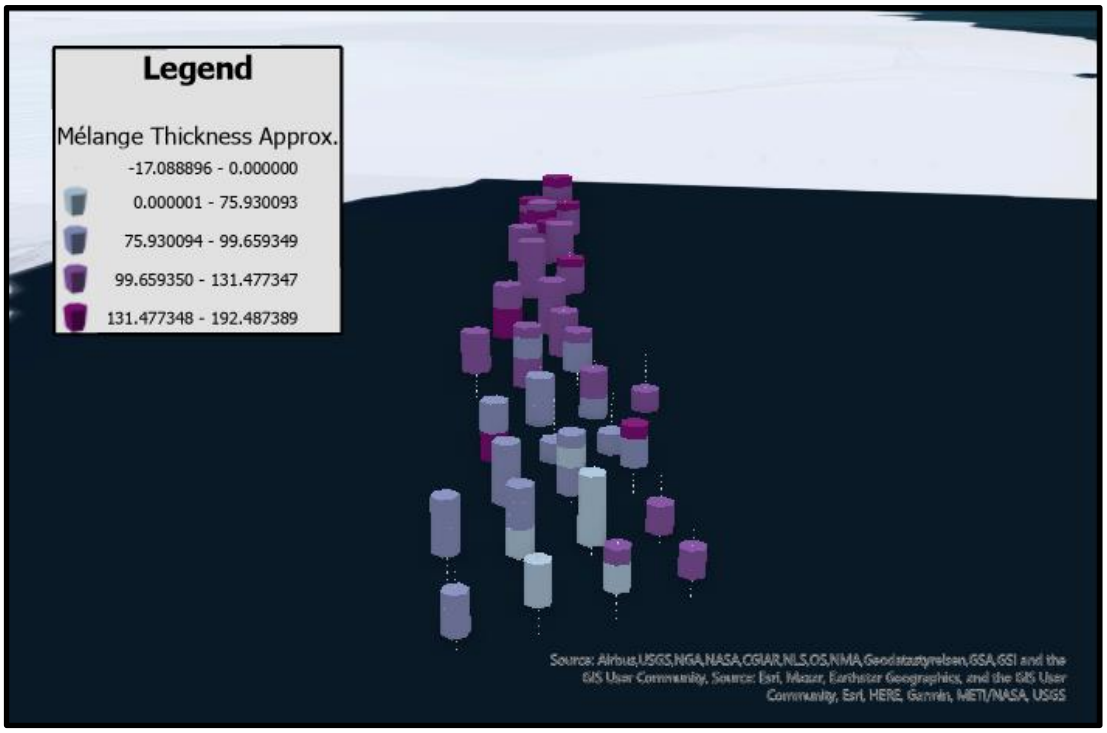

Figure 14: Using the ArcGIS Imagery Basemap in a 3D scene, we provide visual context for how Space-Time Cubes allow us to better assess localized trends in ICESat-2 approximated mélange thickness within a particular rift system, in this case rift L2. Due to the 1000m neighborhood, this is less reliable at narrow rift tips and favors analysis of larger or wider rifts.

the reality of mélange thickness increasing traveling upstream from the ice front. This, coupled with our evidence for longitudinal-to-flow rift propagation being most prevalent at the ice front (Figure 12) further confirmed that mélange thickness functions as a control on overall rift propagation.

4.3.3 Emerging Hot Spot Analysis

While the STC provides additional insight into the structure of each rift system's mélange thickness, it serves primarily as a visual representation from which only some knowledge can be gained. Rather than rely on further human observation to make spatiotemporal claims of trends, we used Emerging Hot Spot (EHS) Analysis to truly assess and characterize the behavior of mélange within a rift and relate this spatiotemporal behavior to the results of rift propagation (longitudinal-to-flow and transverse-to-flow). The tool, provided within ESRI's ArcGIS Pro, utilized the Getis Ord Gi* statistic to determine the p-value and z-score for every bin within the STC and then the Mann-Kendall statistic trends to identify localities of excessive increase or decrease in mélange thickness when compared to the entire rift. The EHS analysis identified regions throughout each rift which had the greatest spatiotemporal variability (Figure 15, page 44).

The smallest rift, L2, had only 3 hotspot locations, although this is consistent with its lower level of activity. Rift T2 saw the greatest variability in EHS categorization implying the mélange surface (which we approximate to thickness) varies most greatly on rift T2, or at least that it has since the 2019 calving event. T2 is also the only rift dominated by transverse-to-flow propagation with an RGM less than 0. Finally, rift E3

saw more hot spots near the rift mouth and windblown rift walls. The mélange thickness approximation for this rift is noticeably thinner than L2 or T2 (Figure 13), however the regions where thickness increases did occur coincide well with the along-track propagation measured by ICESat-2. We also saw some new hot spots identified near the rift tip where mélange thickness was approximated to be thickest, relevant due to E3's high RGM and therefore its tendency toward longitudinal-to-flow propagation at the rift tip. These emerging hot spots allow us to better describe the nature of mélange changes to multidimensional propagation rates, with transverse-to-flow widening rates being typically associated with seasonal mélange behavior and longitudinal-to-flow rates from the rift tip being associated with prevailing mélange increases near the rift tip.

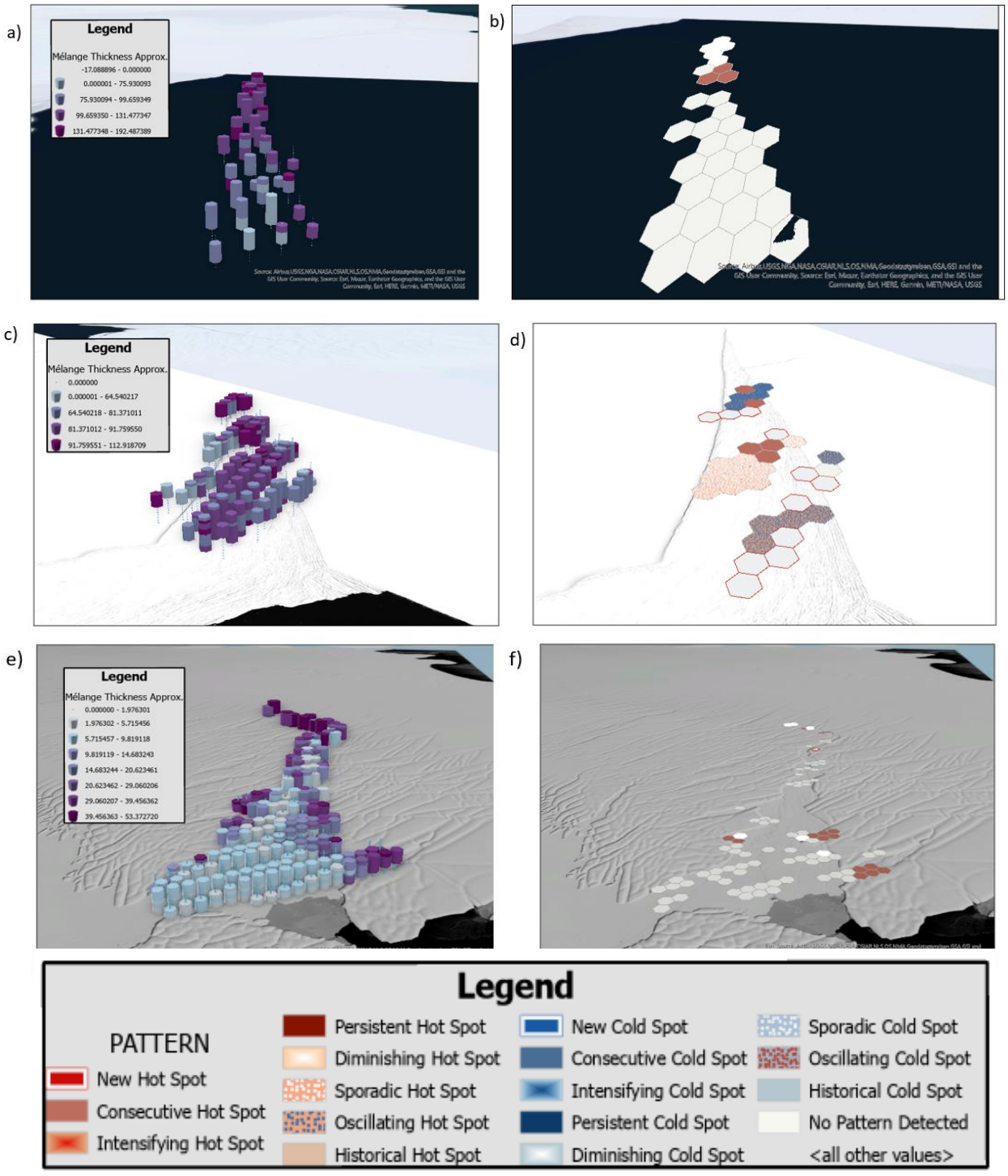

Figure 15: a) The Space-Time cube (STC) for rift L2, b) the Emerging Hot Spot (EHS) results for L2, c) STC for rift T2, d) EHS for rift T2, e) STC for rift E3, f) EHS for rift E3. Looking at the visual context provided by the multidimensional STCs and the results from comparing local neighborhoods of approximated mélange thickness we can see areas which are increasing (either new hot spots or consecutive hot spots) in relation their surrounding neighborhood.

5. Discussion

Ice rifts and the mélange within occur naturally in a steady state system, but increasing presence of rifts and quickening iceberg calving cycles weaken the integrity of ice shelves as a buttress for grounded ice in Antarctica. In our study, ICESat-2 and Landsat 8 data were used in tandem to assess the propagation behavior of three rifts on AIS, as well as to investigate the behavior of the ice mélange matrix on a seasonal time scale. Subsequently, we tested the strength of the correlation between mélange thickness and propagation rate to determine whether or not mélange thickness acts as a control on rift growth. By doing so, we have produced a new method for looking at small-scale ice shelf dynamics, developed a novel metric which we believe may be indicative of a particular rift's imminent propagation to calving, and shown that mélange behavior is well correlated with propagation observations.

5.1 Identifying the primary propagation direction

Rift propagation can occur along two major planes: longitudinal-to-flow (lengthening along the extensional plane) and transverse-to-flow (widening). For most of a rifts' lifecycle, propagation is either dominated by transverse-to-flow propagation, or the two regimes have similar contributions (Bassis et al., 2005; Fricker, Young, et al., 2005; Rignot & MacAyeal, 1998; Walker et al., 2013). However, during the final stages leading up to iceberg calving, propagation events are typically rapid (greater than 50 m per day) and occur longitudinal-to-flow (Bassis et al., 2005; Larour et al., 2004). Our RGM metric enabled us to monitor the relative contribution of propagation in each direction, and numerically define which propagation style is dominating over a given

season. Using this method applied to satellite observations, we were able to determine when longitudinal-to-flow propagation started to dominate the rift dynamics on a seasonal timescale.

All three rifts had relatively similar RGMs before the 2019 calving of iceberg D-28; following that event, there were deviations in propagation behavior between all three rifts (Figure 13). Rift L2 did not experience any significant change, remaining with widthwise and longitudinal-to-flow propagation both remaining below two meters per day and therefore an unchanging RGM, implying that it was not impacted by the calving event. It is also important to note that rift L2 is the least active of the three rifts in our study. Aside from its lower propagation rates which did not exceed more than 2 meters per day over the study period, this reduced activity is also indicated by its dramatically thicker mélange base. The RGM of rift T2 remained below 1.0 and gradually decreased, implying a trend towards widthwise propagation following the calving event, coupled by small mélange thickness increases of less than 3 meters throughout the rift (Figure 15). We assume that this mélange thickness change resulted from the Loose-tooth rift system restabilizing after the calving event, rather than changes that would occur independently from additional snow deposit or refreezing. Finally, rift E3 experienced drastic increases in the longitudinal-to-flow propagation following the event from approximately three meters per day to more than 30 meters per day with the highest rates measured near the end of the melt season each year. This propagation increase was coupled with new high-thickness mélange developing at the rift tip in accordance with the wedge hypothesis (Bassis et al., 2005). We also acknowledge that E3 is currently propagating through a crevasse field, which may allow for rapid propagation as

the E3 connects with each new crevasse. However, the most recent crevasse that E3 propagated into marks the western edge of the crevasse field and the propagation rates have continued steadily (Figure 11). E3 is both the largest (by area) and longest rift on Amery Ice Shelf; consequently, with the dramatic increase in longitudinal-to-flow propagation, we expect the next calving cycle defining event to involve E3. These observations are only possible through the combination of both ICESat-2 altimetric data and Landsat imagery data; together, they provide a multidimensional look and two different propagation planes.

The idea that rift E3 is likely to be involved in the next large scale calving event is drawn from 3 separate observations. First and foremost, E3 is dominated heavily by longitudinal-to-flow propagation at the rift tip. It is likely that this domination is due partly to environmental factors, such as its presence propagating through a crevasse field. With higher roughness and lower ice shelf integrity surrounding rift E3, the rift can behave more actively. Secondly, rift E3 is now propagating into the center of the ice shelf, a much less damaged area. Its nearest rifting neighbor is rift T2. It is unclear if the next calving event would involve T2 or not, but based on the propagation direction and lack of other surrounding rifts, if the direction remained stable until calving, this would lead to a calving event more than double the size of D-28 (Walker et al., 2021). Lastly, the most recent crevasse that became part of E3 is propagating in two places, one to the west (the E3 rift tip) and the other to the east. While this alternative propagation tip is not included in this study, it is propagating back through the crevasse field eastward, creating the potential for multiple calving events (still in the range of 800 square

kilometers or more), implying that regardless of where E3 propagates most quickly, it will be part of the next major calving event on Amery Ice Shelf.

5.2 Local trends in mélange thickness

Mélange forms at the exposed sea level inside ice shelf rifts and develops from many sources. Mélange ultimately thickens beyond its original formation at sea level creating a freeboard that we observe using ICESat-2 and draft which is estimated following Archimedes principle as outlined in our methods. While we acknowledge that mélange is a rheologically complex conglomerate of ice types, there have been no recent measurements of mélange density on Amery Ice Shelf. Early data was used, under the assumption that Amery's classification as "in balance" implies that there have not been large density changes to the ice shelf (W. F. Budd et al., 1982; Rignot et al., 2019). ICESat-2 data, along with advancing GIS software, allowed us to look at the mélange evolution over the study period in small neighborhoods (1000m) and classify the change of each neighborhood with respect to its along-track surroundings. By doing so, we characterized mélange evolution at a small scale, promoting identification of particular locations where mélange thickness changes occurred. While we do not propose any new mechanisms for mélange formation, the method of using spatio-temporal analysis does reveal both the seasonal variation of mélange and the necessity for higher temporal sampling to discover more about mélange behavior. Near the rift tip (landward), we found these thickness changes to be in line with formation processes proposed by the wedge hypothesis, whereas mélange thickness increases near the rift mouth and center are more likely to be driven by collapse of ice blocks and long-term

marine ice growth, and do not necessarily imply faster widening rate. While mélange change on a regular seasonal scale has not been observed conclusively, ICESat-2 altimetry allowed us to gain a seasonal snapshot of the status of mélange on AIS. We observed some seasonal thickness change, likely due to melt runoff, but we were unable to determine any changes at a higher temporal resolution than that.

The results of this study could be expanded using SAR or in situ sensors, similar to those used in previous studies (Bassis et al., 2005). SAR provides the opportunity to penetrate through the cloud cover year-round, with similar temporal resolution, but ICESat-2's accuracy and precision made it a more preferable remote sensing instrument. By maintaining incredibly accurate observations of mélange surfaces and rift walls for propagation estimation, we are able to identify small scale changes and draw conclusions from our results including new mélange behavior trends. Mélange thickness seems to vary most in regions where the propagation (in either direction) is varying greatly, with low propagation regions seeing a decrease in mélange variability. This is further affirmation that mélange does act as a control on rift propagation. While our temporal resolution makes drawing the conclusion of which occurs first, the propagation or the mélange thickness changes, more speculatory, our results verify that they are in fact well correlated.

As mentioned earlier, there are two prevailing theories regarding the relation of mélange thickness. Our results support that mélange thickness increases near the rift tip are associated with longitudinal-to-flow propagation rate increases. This implies that the wedge theory is applicable at the rift tip where brand new mélange is formed by rapid input of water into new free space as propagation occurs (Bassis et al., 2005) on a

seasonal time scale. We also note the presence of greater mélange thickness on the predominant windblown rift wall (southwestern walls) where snow is most likely to accumulate in larger quantities ultimately leading to more firn formation (Leonard et al., 2008). We attribute prevailing mélange thickness trends near the ice front to this windblown build up and to ice block collapse, which (in contrast to the glue theory) is sometimes observed with propagation increases (Larour et al., 2004). However, our observations of seasonal mélange thinning and thickening are in agreement with this study (Figure 13). This discrepancy is evident because the position of the rift mouth hot spots are associated with one side of the rift wall, not because the rift mouth thickness increases directly cause the increase in widening rate. In the case of rift T2, dominated by widening increases (average RGM of 0.34), the rift wall moving most prevalently is the wall associated with thinner mélange which also has less variability. The most significant changes in mélange thickness, as determined by our Emerging Hot Spot Analysis were found on ICESat-2 tracks nearest to the rift mouth or rift tips.

5.3 Describing the relationship between rift growth and mélange thickness change

We utilized the improved spatiotemporal resolution provided by ICESat-2 and Landsat combined with geospatial analysis techniques to advance current understanding of the relationship between rift growth and mélange thickness in three rifts on AIS. Rift L2 is the smallest rift of the three with an average rift length of 15.1 km. L2 does have the greatest mélange thickness, but also maintained the lowest overall propagation rates throughout the study period with the lowest varying RGM, as well as

had the fewest hotspots of mélange thickness increase. Rift T2 is the middle rift in this study with an average rift length of 25.6 km. T2 has the most active mélange of the three rifts investigated and has the lowest RGM trending towards widthwise propagation more than longitudinal-to-flow. This rift was closest in proximity to the D28 calving event, but mélange thickness increases were still noted along the windblown wall and especially near the rift mouth. Rift E3 is the largest rift investigated at 67.3 km and is also coupled with the largest variation in mélange thickness from tip to mouth as well as the greatest change in RGM over the course of the study period (Leonard et al., 2008) and the thinnest mélange. It was extremely active following the D-28 calving event with the lower bound of lengthwise propagation over 50 meters per day the following year (overall rate decreasing annually). This is further confirmation that E3 will likely be involved in the next major calving event. Elaborating on the differences and similarities between each of the three rifts included in this study, we found that each rift differed in physical characteristics (overall mélange thickness, rift size, propagation rates) while behaving accordingly with the mélange thickness changes observed by ICESat-2.

Ultimately, rifts T2 and E3 had transverse-to-flow propagation rates with spatiotemporal mélange thickness increases occurring along the same tracks that increasing propagation rates were observed near the rift tip and rift mouth. Mélange increases near the rift tip in rift E3 were associated with accelerated longitudinal-to-flow propagation, while increases near the rift mouth were most consistently indicative of formation increases along a single rift wall, then throughout the entire rift. We also found high mélange thickness observations near rift tips seasonally, which is indicative of the wedge mechanism proposed by Bassis et al., 2005. This implication also assumes the

mechanism is applicable on a seasonal time scale with a longer study period, rather than a shorter but higher resolution study period as used in the original investigation. Widening at the rift mouth is more likely due to the seasonal thickening and thinning of mélange allowing one rift wall to move more freely (Larour et al., 2004). While we did discern some prevailing hot spots of mélange thickness, especially near the rift mouths, our hot spot analysis identified changes throughout the two more active rifts and our hot spot analysis did not reveal any significant cold spots (locations of prevailing mélange thickness decreases). This could be due to the spatial resolution of ICESat-2 tracks or could imply that the overall formation of mélange is outpacing the melt and degradation on Amery Ice Shelf.

6. Summary and Future Work

Our study focused on investigating three continuously active rifts on Amery Ice Shelf using ICESat-2 and Landsat 8 Imagery. The research objectives were to determine: (i) the possibility of characterizing the primary propagation style of Antarctic ice rifts, (ii) if mélange exists uniformly and determine the time scale on which it behaves, and (iii) the influence of rift mélange on rift growth.

Through our analysis, we incorporated observations from both satellites to identify a primary propagation direction for the rifts. By introducing the Rift Growth Metric (RGM), we have provided a novel metric to describe propagation style (longitudinal-to-flow or transverse-to-flow), proving that rift T2 is dominated heavily by transverse-to-flow propagation and E3 is dominated heavily by longitudinal-to-flow propagation). Furthermore, our findings revealed that rift mélange is not uniform in ice front rifts and exhibits subtle seasonal variation. We also provided further cadence to the notion that local mélange thickening is consistent with mélange involvement in initial ice rift growth by categorizing the spatiotemporal variation of 1000m mélange neighborhoods.

During the study period, the intermittent presence of clouds inhibited data acquisition for both satellites. To mitigate this, we extended the definition of successive observations for transverse-to-flow propagation (measured by ICESat-2) and relied on adjusted gamma values for manual measurements in imagery (captured by Landsat 8). Additionally, ICESat-2 has a footprint size of only 13 ft. Increasing the observation footprint size or amount of laser beams used could improve our knowledge of the system and allow for the production of seasonal (or better) DEMs, thus expanding the

availability of mélange observations. In situ deployment of sensors within the mélange base of rifts via airdrop and the use of additional remote sensing data from Synthetic Aperture Radar (SAR) and regular airborne LiDAR observations could further enhance our understanding of mélange dynamics.

Our study on the highly active and variable rift system of Amery Ice Shelf has significantly advanced our knowledge of rift growth parameters in the Antarctic. Additionally, we introduced a new method for visualizing and analyzing altimetric data, highlighting the relevance of ICESat-2 and emphasizing the need for higher temporal sampling to improve our understanding of ice shelf calving cycles. The insights gained from our findings have important implications for improving mass balance models and enhancing our understanding of ice shelf processes.

In conclusion, this study contributes to the body of knowledge on Antarctic rifts and their interaction with mélange while establishing a new metric for quantifying rift propagation behavior. Further research using advanced remote sensing techniques and in situ observations can build upon our findings and deepen our understanding of this complex system.

7. References

Adusumilli, S., Fish, M., Fricker, H. A., & Medley, B. (2021). Atmospheric River Precipitation Contributed to Rapid Increases in Surface Height of the West Antarctic Ice Sheet in 2019. *Geophysical Research Letters*, *48*(5). https://doi.org/10.1029/2020GL091076

Adusumilli, S., Fricker, H. A., Medley, B., Padman, L., & Siegfried, M. R. (2020). Interannual variations in meltwater input to the Southern Ocean from Antarctic ice shelves. *Nature Geoscience*, *13*(9), 616–620. https://doi.org/10.1038/s41561-020-0616-z

Alley, K. E., Scambos, T. A., Siegfried, M. R., & Fricker, H. A. (2016). Impacts of warm water on Antarctic ice shelf stability through basal channel formation. *Nature Geoscience*, *9*(4), 290–293. https://doi.org/10.1038/ngeo2675

Bassis, J. N., Coleman, R., Fricker, H. A., & Minster, J. B. (2005). Episodic propagation of a rift on the Amery Ice Shelf, East Antarctica. *Geophysical Research Letters*, *32*(6), L06502. https://doi.org/10.1029/2004GL022048

Brenner, A. C., DiMarzio, J. P., & Zwally, H. J. (2007). Precision and Accuracy of Satellite Radar and Laser Altimeter Data Over the Continental Ice Sheets. *IEEE Transactions on Geoscience and Remote Sensing*, *45*(2), 321–331. https://doi.org/10.1109/TGRS.2006.887172

Brunt, K. M., Neumann, T. A., & Smith, B. E. (2019). Assessment of ICESat-2 Ice Sheet Surface Heights, Based on Comparisons Over the Interior of the Antarctic Ice Sheet. *Geophysical Research Letters*, *46*(22), 13072–13078. https://doi.org/10.1029/2019GL084886

Budd, W. (1966). The Dynamics of the Amery Ice Shelf. *Journal of Glaciology*, *6*(45), 335–358. https://doi.org/10.3189/S0022143000019456

Budd, W. F., Corry, M. J., & Jacka, T. H. (1982). Results From The Amery Ice Shelf Project. *Annals of Glaciology*, *3*, 36–41. https://doi.org/10.3189/S0260305500002494

Cheng, Y., Xia, M., Qiao, G., Li, Y., Hai, G., & Lv, D. (2021). Calving cycle of Ninnis Glacier over the last 60 years. *International Journal of Applied Earth Observation and Geoinformation*, *105*, 102612. https://doi.org/10.1016/j.jag.2021.102612

De Rydt, J., Gudmundsson, G. H., Nagler, T., & Wuite, J. (2019). Calving cycle of the Brunt Ice Shelf, Antarctica, driven by changes in ice shelf geometry. *The Cryosphere*, *13*(10), 2771–2787. https://doi.org/10.5194/tc-13-2771-2019

Dow, C. F., Lee, W. S., Greenbaum, J. S., Greene, C. A., Blankenship, D. D., Poinar, K., Forrest, A. L., Young, D. A., & Zappa, C. J. (2018). Basal channels drive active surface hydrology and transverse ice shelf fracture. *Science Advances*, *4*(6), eaao7212. https://doi.org/10.1126/sciadv.aao7212

Dupont, T. K., & Alley, R. B. (2005). Assessment of the importance of ice-shelf buttressing to ice-sheet flow: BUTTRESSING SENSITIVITY. *Geophysical Research Letters*, *32*(4),

n/a-n/a. https://doi.org/10.1029/2004GL022024

Fretwell, P., Pritchard, H. D., Vaughan, D. G., Bamber, J. L., Barrand, N. E., Bell, R., Bianchi, C., Bingham, R. G., Blankenship, D. D., Casassa, G., Catania, G., Callens, D., Conway, H., Cook, A. J., Corr, H. F. J., Damaske, D., Damm, V., Ferraccioli, F., Forsberg, R., Gujita, S., Gim Y., Gogineni P., Griggs J. A., Hindmarsh R. C. A., Holmund P., Holt J. W., Jacobel R. W., Jenkins, A., Jokat, W., Jordan, T., King, E. C., Kohler, J., Krabill, W., Riger-Kusk, M., Langley, K. A., Leitchenkov, G, Leucschen, C., Luyendyk, B. ., Matsuoka, K., Mouginot, J., Nitsche, F. O., Nogi, Y., Nost, O. A., Popov, S. V., Rignot, E., Rippin, D. M., Rivera, A., Roberts, J., Ross, N., Siegert, M. J., Smith, A. M., Steinhage, D., Studinger, M., Sun, B., Tinto, B. K., Welch, B. C., Wilson, D., Young, D. A., Xangbin, C., and Zirizzotti, A. (2013). Bedmap2: Improved ice bed, surface and thickness datasets for Antarctica. *The Cryosphere*, *7*(1), 375–393. https://doi.org/10.5194/tc-7-375-2013

Fricker, H. A., Bassis, J. N., Minster, B., & MacAyeal, D. R. (2005). ICESat's new perspective on ice shelf rifts: The vertical dimension. *Geophysical Research Letters*, *32*(23). https://doi.org/10.1029/2005GL025070

Fricker, H. A., Popov, S., Allison, I., & Young, N. (2001). Distribution of marine ice beneath the Amery Ice Shelf. *Geophysical Research Letters*, *28*(11), 2241–2244. https://doi.org/10.1029/2000GL012461

Fricker, H. A., Young, N. W., Allison, I., & Coleman, R. (2002). Iceberg calving from the Amery Ice Shelf, East Antarctica. *Annals of Glaciology*, *34*, 241–246. https://doi.org/10.3189/172756402781817581

Fricker, H. A., Young, N. W., Coleman, R., Bassis, J. N., & Minster, J.-B. (2005). Multi-year monitoring of rift propagation on the Amery Ice Shelf, East Antarctica. *Geophysical Research Letters*, *32*(2), L02502. https://doi.org/10.1029/2004GL021036

Gudmundsson, G. H., Paolo, F. S., Adusumilli, S., & Fricker, H. A. (2019). Instantaneous Antarctic ice sheet mass loss driven by thinning ice shelves. *Geophysical Research Letters*, *46*(23), 13903–13909. https://doi.org/10.1029/2019GL085027

Hambrey, M. J., & Dowdeswell, J. A. (1994). Flow regime of the Lambert Glacier-Amery Ice Shelf system, Antarctica: Structural evidence from Landsat imagery. *Annals of Glaciology*, *20*, 401–406. https://doi.org/10.3189/1994AoG20-1-401-406

Joughin, I., Smith, B. E., & Medley, B. (2014, May 16). *Marine Ice Sheet Collapse Potentially Under Way for the Thwaites Glacier Basin, West Antarctica | Science*. https://www.science.org/doi/10.1126/science.1249055

King, M. A., Coleman, R., Freemantle, A.-J., Fricker, H. A., Hurd, R. S., Legrésy, B., Padman, L., & Warner, R. (2009). A 4-decade record of elevation change of the Amery Ice Shelf, East Antarctica. *Journal of Geophysical Research: Earth Surface*, *114*(F1). https://doi.org/10.1029/2008JF001094

Larour, E., Rignot, E., & Aubry, D. (2004). Modelling of rift propagation on Ronne Ice Shelf, Antarctica, and sensitivity to climate change. *Geophysical Research Letters*, *31*(16).

https://doi.org/10.1029/2004GL020077

Larour, E., Rignot, E., Poinelli, M., & Scheuchl, B. (2021). Physical processes controlling the rifting of Larsen C Ice Shelf, Antarctica, prior to the calving of iceberg A68. *Proceedings of the National Academy of Sciences*, *118*(40), e2105080118. https://doi.org/10.1073/pnas.2105080118

Lauer, D. T. (1997). *The Landsat Program: Its Origins, Evolution, and Impacts*.

Lenaerts, J. T. M., Medley, B., van den Broeke, M. R., & Wouters, B. (2019). Observing and Modeling Ice Sheet Surface Mass Balance. *Reviews of Geophysics (Washington, D.C. : 1985)*, *57*(2), 376–420. https://doi.org/10.1029/2018RG000622

Leonard, K. C., Tremblay, L.-B., MacAyeal, D. R., & Jacobs, S. S. (2008). Interactions of wind-transported snow with a rift in the Ross Ice Shelf, Antarctica. *Geophysical Research Letters*, *35*(5). https://doi.org/10.1029/2007GL033005

Ligtenberg, S. R. M., Helsen, M. M., & van den Broeke, M. R. (2011). An improved semi-empirical model for the densification of Antarctic firn. *The Cryosphere*, *5*(4), 809–819. https://doi.org/10.5194/tc-5-809-2011

Lipovsky, B. P. (2020). Ice shelf rift propagation: Stability, three-dimensional effects, and the role of marginal weakening. *The Cryosphere*, *14*(5), 1673–1683. https://doi.org/10.5194/tc-14-1673-2020

Luthcke, S. B., Thomas, T. C., Pennington, T. A., Rebold, T. W., Nicholas, J. B., Rowlands, D. D., Gardner, A. S., & Bae, S. (2021). ICESat-2 Pointing Calibration and Geolocation Performance. *Earth and Space Science*, *8*(3), e2020EA001494. https://doi.org/10.1029/2020EA001494

Marsh, O. J., Fricker, H. A., Siegfried, M. R., Christianson, K., Nicholls, K. W., Corr, H. F. J., & Catania, G. (2016). High basal melting forming a channel at the grounding line of Ross Ice Shelf, Antarctica. *Geophysical Research Letters*, *43*(1), 250–255. https://doi.org/10.1002/2015GL066612

Morlighem, M., Rignot, E., Binder, T., Blankenship, D., Drews, R., Eagles, G., Eisen, O., Ferraccioli, F., Forsberg, R., Fretwell, P., Goel, V., Greenbaum, J. S., Gudmundsson, H., Guo, J., Helm, V., Hofstede, C., Howat, I., Humbert, A., Jokat, W., Karlsson, B. N., Lee, W. S., Matsouka, K., Millan, R., Mouginot, J., Paden, J., Pattyn, F., Roberts, J., Rosier, S., Ruppel, A., Seroussi, H., Smith, E. C., Steinhage, D., Sun, B., van den Broeke, M. R., van Ommen, T. D., van Wessem, M., and Young, D. A. (2020). Deep glacial troughs and stabilizing ridges unveiled beneath the margins of the Antarctic ice sheet. *Nature Geoscience*, *13*(2), Article 2. https://doi.org/10.1038/s41561-019-0510-8

Paolo, F. S., Fricker, H. A., & Padman, L. (2015). Volume loss from Antarctic ice shelves is accelerating. *Science*, *348*(6232), 327–331. https://doi.org/10.1126/science.aaa0940

Phillips, H. A. (1999). *Applications of ERS satellite radar altimetry in the Lambert Glacier-Amery Ice Shelf system, East Antarctica*.

Pritchard, H. D., Ligtenberg, S. R. M., Fricker, H. A., Vaughan, D. G., van den Broeke, M. R., & Padman, L. (2012). Antarctic ice-sheet loss driven by basal melting of ice shelves. *Nature*, *484*(7395), 502–505. https://doi.org/10.1038/nature10968

Rignot, E., Jacobs, S., Mouginot, J., & Scheuchl, B. (2013). Ice-Shelf Melting Around Antarctica. *Science*, *341*(6143), 266–270. https://doi.org/10.1126/science.1235798

Rignot, E., & MacAyeal, D. R. (1998). Ice-shelf dynamics near the front of the Filchner—Ronne Ice Shelf, Antarctica, revealed by SAR interferometry. *Journal of Glaciology*, *44*(147), 405–418. https://doi.org/10.3189/S0022143000002732

Rignot, E., Mouginot, J., Scheuchl, B., van den Broeke, M., van Wessem, M. J., & Morlighem, M. (2019). Four decades of Antarctic Ice Sheet mass balance from 1979–2017. *Proceedings of the National Academy of Sciences*, *116*(4), 1095–1103. https://doi.org/10.1073/pnas.1812883116

Seroussi, H., Nowicki, S., Payne, A. J., Goelzer, H., Lipscomb, W. H., Abe-Ouchi, A., Agosta, C., Albrecht, T., Asay-Davis, X., Barthel, A., Calov, R., Cullather, R., Dumas, C., Galton-Fenzi, B. K., Gladstone, R., Golledge, N. R., Gregory, J. M., Greve, R., Hattermann, T., Hoffman, M. J., Humbert, A., Huybrechts, P., Jourdain, N. C., Kleiner, T., Larour, E., Leguy, G. R., Lowry, D. P., Little, C. M., Morlighem, M., Pattyn, F., Pelle, T., Price, S. F., Quiquet, A., Reese, R., Schlegel, N.-J., Shepherd, A., Simon, E., Smith, R. S., Straneo, F., Sun, S., Trusel, L. D., Van Breedam, J., van de Wal, R. S. W., Winkelmann, R., Zhao, C., Zhang, T., and Zwinger, T.: ISMIP6 Antarctica: a multi-model ensemble of the Antarctic ice sheet evolution over the 21st century, The Cryosphere, 14, 3033–3070, https://doi.org/10.5194/tc-14-3033-2020, 2020.

Shen, Q., Wang, H., Shum, C. K., & Jiang, L. (2020). *Antarctic-Wide Annual Ice Flow Maps from Landsat 8 Imagery between 2013 and 2019* [dataset]. PANGAEA. https://doi.org/10.1594/PANGAEA.914253

Smith, B., Fricker, H. A., Gardner, A. S., Medley, B., Nilsson, J., Paolo, F. S., Holschuh, N., Adusumilli, S., Brunt, K., Csatho, B., Harbeck, K., Markus, T., Neumann, T., Siegfried, M. R., & Zwally, H. J. (2020). Pervasive ice sheet mass loss reflects competing ocean and atmosphere processes. *Science*, *368*(6496), 1239–1242. https://doi.org/10.1126/science.aaz5845

Smith, B., H. A. Fricker, A. Gardner, M. R. Siegfried, S. Adusumilli, B. M. Csathó, N. Holschuh, J. Nilsson, F. S. Paolo, and the ICESat-2 Science Team. 2020. *ATLAS/ICESat-2 L3A Land Ice Height, Version 5*. Boulder, Colorado USA. NASA National Snow and Ice Data Center Distributed Active Archive Center. doi: https://doi.org/10.5067/ATLAS/ATL06.005. [10/23/2022].

Smith, B., Fricker, H. A., Holschuh, N., Gardner, A. S., Adusumilli, S., Brunt, K. M., Csatho, B., Harbeck, K., Huth, A., Neumann, T., Nilsson, J., & Siegfried, M. R. (2019). Land ice height-retrieval algorithm for NASA's ICESat-2 photon-counting laser altimeter. *Remote Sensing of Environment*, *233*, 111352. https://doi.org/10.1016/j.rse.2019.111352

Spergel, J. J., Kingslake, J., Creyts, T., van Wessem, M., & Fricker, H. A. (2021). Surface meltwater drainage and ponding on Amery Ice Shelf, East Antarctica, 1973–2019.

Journal of Glaciology, *67*(266), 985–998. https://doi.org/10.1017/jog.2021.46

Swithinbank, C. (1988). *Satellite image atlas of glaciers of of the world—Antarctica* (R. S. Williams & J. G. Ferrigno, Eds.; Vol. 1386B). Unites States Government Printing Office. http://dx.doi.org/10.3133/pp1386B

Tinto, K. J., Padman, L., Siddoway, C. S., Springer, S. R., Fricker, H. A., Das, I., Caratori Tontini, F., Porter, D. F., Frearson, N. P., Howard, S. L., Siegfried, M. R., Mosbeux, C., Becker, M. K., Bertinato, C., Boghosian, A., Brady, N., Burton, B. L., Chu, W., Cordero, S. I., Dhakal, T., Dong, L., Gustafson, C. D., Keeshin, S., Locke, C., Lockett, A., O'Brien, G., Spergel, J. J., Starke, S. E., Tankersley, M., Wearing, M. G., and Bell, R. E. (2019). Ross Ice Shelf response to climate driven by the tectonic imprint on seafloor bathymetry. *Nature Geoscience*, *12*(6), 441–449. https://doi.org/10.1038/s41561-019-0370-2

United States Geological Survey (USGS). (2018-2022). Landsat 8-9 OLI/TIRS Collection 2 Level-2 Data. DOI: 10.5066/P9OGBGM6

Vaughan, D.G., J.C. Comiso, I. Allison, J. Carrasco, G. Kaser, R. Kwok, P. Mote, T. Murray, F. Paul, J. Ren, E. Rignot, O. Solomina, K. Steffen and T. Zhang, 2013: Observations: Cryosphere. In: Climate Change 2013: The Physical Science Basis. Contribution of Working Group I to the Fifth Assessment Report of the Intergovernmental Panel on Climate Change [Stocker, T.F., D. Qin, G.-K. Plattner, M. Tignor, S.K. Allen, J. Boschung, A. Nauels, Y. Xia, V. Bex and P.M. Midgley (eds.)]. Cambridge University Press, Cambridge, United Kingdom and New York, NY, USA.

Walker, C. C., Bassis, J. N., Fricker, H. A., & Czerwinski, R. J. (2013). Structural and environmental controls on Antarctic ice shelf rift propagation inferred from satellite monitoring. *Journal of Geophysical Research: Earth Surface*, *118*(4), 2354–2364. https://doi.org/10.1002/2013JF002742

Walker, C. C., Becker, M. K., & Fricker, H. A. (2021). A High Resolution, Three-Dimensional View of the D-28 Calving Event From Amery Ice Shelf With ICESat-2 and Satellite Imagery. *Geophysical Research Letters*, *48*(3). https://doi.org/10.1029/2020GL091200

Walker, C. C., & Gardner, A. S. (2019). Evolution of ice shelf rifts: Implications for formation mechanics and morphological controls. *Earth and Planetary Science Letters*, *526*, 115764. https://doi.org/10.1016/j.epsl.2019.115764

Whiteford, A., Horgan, H., Leong, W. J., & Forbes, M. (2022). Melting and Refreezing in an Ice Shelf Basal Channel at the Grounding Line of the Kamb Ice Stream, West Antarctica. *Journal of Geophysical Research: Earth Surface*, *127*. https://doi.org/10.1029/2021JF006532

Xu, D., Tang, X., Yang, S., Zhang, Y., Wang, L., Li, L., & Sun, B. (2022). Revisiting Ice Flux and Mass Balance of the Lambert Glacier–Amery Ice Shelf System Using Multi-Remote-Sensing Datasets, East Antarctica. *Remote Sensing*, *14*(2), Article 2. https://doi.org/10.3390/rs14020391